

NEW TWO-COLOR DIMER MODELS WITH CRITICAL GROUND STATES

R. Raghavan, Christopher L. Henley,* Scott L. Arouh †
Laboratory of Atomic and Solid State Physics
Ithaca, NY 14853-2501

Received

ABSTRACT: We define two new models on the square lattice, in which each allowed configuration is a superposition of a covering by “white” dimers and one by “black” dimers. Each model maps to a solid-on-solid (SOS) model in which the “height” field is two dimensional. Measuring the stiffness of the SOS fluctuations in the rough phase provides critical exponents of the dimer models. Using this “height” representation, we have performed Monte Carlo simulations. They confirm that each dimer model has critical correlations and belongs to a new universality class. In the “dimer-loop” model (which maps to a loop model) one height component is smooth but has unusual correlated fluctuations; the other height component is rough. In the “noncrossing-dimer” model, the heights are rough having two different elastic constants; an unusual form of its elastic theory implies anisotropic critical correlations.

1. INTRODUCTION

Certain discrete spin models are defined by a constraint on the configurations, with all allowed configurations receiving equal statistical weights. Among these are dimer models and ice models, as well as the (highly degenerate) ground state ensembles of antiferromagnetic Potts models and frustrated Ising models. Many of the models on two-dimensional lattices are critical, in that correlation functions decay with distance as power laws [1]; and every one of these critical models has been found to have a “height representation” [2,3], that is, a 1-to-1 mapping of the microstates to those of a sort of interface model.

A “height representation” means that each configuration can be mapped to a configuration of “heights” $z(\mathbf{x})$ on the lattice, i.e. to a configuration of a sort of solid-on-solid (SOS) model. Furthermore, this SOS model is (usually) in a rough phase, described at long wavelengths by a gradient-squared elastic free energy. From this we follow a route familiar in the context of the two-dimensional XY model [4]: the height fluctuations diverge logarithmically. Furthermore, local spin operators can be represented as complex exponentials of the height variables. Hence the correlations of those operators decay as the exponential of a logarithm, explaining the criticality and providing formulas for the critical exponents in terms of the elastic constants [5]. (See Sec. 2.1 and 2.5, below, for more about this derivation). The height approach also yields the critical exponents of the specific heat and correlation length as $T \rightarrow 0$ in models where the excitations map to topological defects of the interface model.

It is possible for the “height” variable $\mathbf{z}(\mathbf{x})$ to have dimensionality $d^\perp > 1$, so that each configuration corresponds to a 2-dimensional surface embedded in a $(2 + d^\perp)$ -dimensional hyperspace. After this point was noticed [3,6], it was a natural step to construct new models which admit height mappings, in the hopes that the heights would be “rough” and the corresponding spin models would be critical. Since only one model with $d^\perp > 1$ was solved in the past (the 3-coloring of the honeycomb lattice [6,7,8]), it is likely that new models of this type belong to new universality classes. For example, Read [9] conjectured that the 4-coloring of a square lattice (which has $d^\perp = 3$) would belong to the universality class of the SU(4) Wess-Zumino-Witten field theory; this has been supported by Monte Carlo simulations [10]. The triangular Ising antiferromagnet, for any spin number $S > 1/2$, is a height model with S -dependent exponents; in this case $d^\perp = 1$ [11]. (The

* To whom correspondence should be addressed

† Current address: Dept. of Physics, Univ. of California San Diego, La Jolla CA 92037

constrained 4-state Potts antiferromagnet on the square lattice, a case where $d^\perp = 5$, was also studied, but in that model the height field appears to be smooth [12].) In some special cases the “height” approach allows the exact determination of an exponent [2,13].

The “height model” approach is closely similar to the “Coulomb gas” theory of critical models [14]. There are three differences in emphasis:

(i) Our “height space” may have more than one dimension. (In Coulomb gas language, there may be more than one flavor of “charge”.)

(ii) We limit ourselves to mappings that are one-to-one between the microscopic spin configurations and the microscopic height configurations, modulo some global arbitrary choices (such as a constant shift of all the heights); the Coulomb gas picture is often applied to less trivial transformations of the partition function, in which additional variables are introduced (and the original variables may be summed over, as in a duality transformation).

(iii) Because the mappings are one-to-one, the height representation can be directly used to analyze Monte Carlo simulations.

Here, we report two models representing two new universality classes. Each model is built from two (interacting) copies of the dimer covering of a square lattice, and each corresponds to $d^\perp = 2$.

1.1 Definitions of the models

The building block for both of our models is the complete covering of a square lattice by dimers (i.e. each vertex has one end of a dimer), as in Fig. 1(a), which will be called the “simple dimer model” in this paper. It is a height model with $d^\perp = 1$, and the elastic constant is known since the model is exactly solved [15]. The new models are:

(i) “Dimer-loop model”. Each allowed configuration consists of “black” dimers, forming a complete dimer covering of the square lattice, and “white” dimers forming another complete dimer covering. We exclude any configurations in which the same bond is occupied by both black and a white dimer; thus the dimers form non-intersecting loops covering all vertices, each loop consisting of alternating white and black dimers (see Fig. 1(b)).

(ii) “Noncrossing dimer model”. Each allowed configuration consists of “black” dimers, forming a complete dimer covering of the square lattice, and “white” dimers forming a complete dimer covering its *dual* lattice. Now, we exclude any configurations in which a white dimer crosses a black dimer (see Fig. 1(d)).

In either model, it can be checked immediately that the interaction between colors is not so strong as to make the models trivial: that is, given a typical configuration of (say) black dimers, there is still an extensive entropy of allowed ways to arrange the white dimers.

Mappings of the dimer-loop model

As its name implies, the dimer-loop model may also be viewed as a loop model, in a family which also contains the equal-weighted six-vertex model. This is useful, firstly because it makes contact with the large literature on loop models and secondly because it suggests concrete interpretations of the two components of the height space (see Sec. 2.3, below).

Take each microstate in this model and make all dimers the same color. The new ensemble contains all ways to cover the sites with nonintersecting loops, each site being covered by exactly one loop, with a fugacity $n = 2$ for each loop (from the two ways in which it could have been colored). This is the square lattice version of the “fully-packed loop” (FPL) model, which was originally defined on the honeycomb lattice [7]. The square lattice FPL model is related to the dimer-loop model in much the same way that the honeycomb FPL model is related to the honeycomb 3-coloring model [8]. The case $n = 1$ of the square lattice FPL model is equivalent to the 6-vertex (square ice) model with every configuration weighted equally [16]. The logic of [7] suggests that the dimer-loop model maps to some $O(n)$ model; it would not be surprising if our case ($n = 2$) were exactly soluble and had rational exponents.

1.2 Outline of the paper

In Sec. 2 (see also the Appendix), we review the basic notions of the theory of height models, as applied to the two-color dimer models: the height representation itself, the special microstates called “ideal states” which are flat in the height representation, the elastic theory, and finally the calculation of critical exponents. Sec. 3 describes the Monte Carlo simulations of both of the two-color dimer models; in addition, we simulated the exactly solved simple dimer model and the BCSOS model as tests. The results are collected in Sec. 4: we found that in the “dimer-loop model”, one component of height space remains rough, while the other component becomes smooth (but with anomalous correlations suggesting a mediated interaction); in the “noncrossing-dimer” model, both components of height space are rough. Sec. 5 contains a summary, some remarks on the new Monte Carlo methods introduced in this work (and Refs. [10-13]), and speculations on possible analytic extensions of this work.

2. HEIGHT REPRESENTATIONS

This section contains the theoretical apparatus for describing the two-color dimer models. As a motivation, it begins by reviewing how all critical exponents can be derived from the elastic constants, in a generic height model. The rest of the section works out the necessary modification for the special cases of the two-color dimer models, with the complications of a two-dimensional height space.

2.1 Fluctuations and correlation functions in height models

Consider a generic height model with (for now) one component in the height space. The microscopic heights $\{z(\mathbf{x})\}$ are defined on each lattice site, and they are coarse grained so as to define a continuous height field $h(\mathbf{x})$. As noted above, the height fluctuations are usually “rough”; here this will mean that the fluctuations of $h(\mathbf{x})$ are weighted according to a gradient-squared elasticity, $F = \int d^2\mathbf{x} f(\nabla h(\mathbf{x}))$, with a free energy density

$$f(\nabla h) = \frac{1}{2}K|\nabla h|^2. \quad (2.1)$$

Inserting (2.1) into a Fourier transform gives

$$F = \sum_{\mathbf{p}} \frac{1}{2}K|\mathbf{p}|^2|h(\mathbf{p})|^2. \quad (2.2)$$

Hence by equipartition,

$$\langle |h(\mathbf{p})|^2 \rangle = \frac{1}{K|\mathbf{p}|^2}. \quad (2.3)$$

From (2.3) we can calculate the height correlation function $C(\mathbf{x}) \equiv \langle [h(\mathbf{x}) - h(0)]^2 \rangle$,

$$C(\mathbf{x}) = \int \frac{d^2\mathbf{p}}{(2\pi)^2} \frac{2(1 - \cos(\mathbf{p} \cdot \mathbf{x}))}{K|\mathbf{p}|^2}. \quad (2.4)$$

$$\simeq \text{const} + \frac{1}{\pi K} \ln |\mathbf{x}|. \quad (2.5)$$

Using (2.5), we can infer the correlation functions of any operator $O(\mathbf{x})$ which is a local function of the spins (or dimers) in the vicinity of \mathbf{x} . First, as will be justified in Sec. 2.2, we can write $O(\mathbf{x}) \approx \tilde{O}(h(\mathbf{x}))$ where $\tilde{O}(h)$ is a periodic function dominated by

$$\tilde{O}(h) \sim \exp(\pm iG^\perp h(\mathbf{x})) \quad (2.6)$$

Then

$$\langle O(\mathbf{x})O(\mathbf{0}) \rangle \sim \text{Re}\langle \exp(iX) \rangle$$

where $X = G^\perp(h(\mathbf{x}) - h(\mathbf{O}))$. But $\langle \exp(iX) \rangle = \exp(-\frac{1}{2}\langle X^2 \rangle)$, since (2.2) implies X is a Gaussian random variable (more precisely, the long-wavelength contribution is). Hence

$$\langle O(\mathbf{x})O(\mathbf{O}) \rangle \sim \exp(-\frac{1}{2}G^2C(\mathbf{x})) \sim r^{-\eta(G^\perp)}, \quad (2.7)$$

where

$$\eta(G^\perp) = \frac{1}{2\pi K}G^{\perp 2} \quad (2.8)$$

In some models, we can admit a small density of topological defect excitations characterized by a Burgers vector b . (That is, if we follow the value of $h(\mathbf{x})$ along a path circling the defect clockwise, then $\mathbf{h}(\mathbf{x})$ is not well-defined but has a net change of b .) The correlation between the defects and antidefects define another kind of correlation function, with “vortex” exponents given by

$$\eta_v(b) = \frac{K}{2\pi}b^2 \quad (2.9)$$

In the case of dimer models, the defects are uncovered (or multiply covered) sites.

Thus, if we know the value of K and the allowed values of G^\perp and b , then eqs. (2.8) and (2.9) provide all the critical exponents that may occur in the model. This was worked out in detail for the case of the triangular Ising antiferromagnet by Blöte, Hilhorst, and Nienhuis [5].

2.2 Ideal states

It is convenient to analyze height models by identifying special “ideal states”, which are microstates in which the configurations are periodic in real space [2,3,10,11,12]. So far, this notion does not have any rigorous basis, but it is a useful shortcut for identifying the “repeat lattice” in height space. The possible Burgers vectors \mathbf{b} of defects (entering eq. (2.9)) belong to the repeat lattice, while the allowed wavevectors \mathbf{G}^\perp (entering eq. (2.8)) of the operators belong to its reciprocal lattice. Hence knowing the repeat lattice and the elastic constants means knowing the possible critical exponents of the model.

Ideal states can be identified by either of the following criteria:

- (i). Flatness: the variance of $\{\mathbf{z}(\mathbf{x})\}$ within the ideal state is minimal.*
- (ii). Entropy: define two microstates to be “neighbors” in configuration space if they differ from each other on the minimum number of sites. (Such minimum differences are shown in Fig. 2). Then an ideal state is one which has the maximum number of neighboring microstates. (That is, of all configurations, the ideal states have the maximum density of sites at which a minimal rearrangement can be performed.) Typically, the same microstates satisfy both criteria.

Each height model has several degenerate ideal states related by symmetry operations. Every ideal state is associated with a “height” $\bar{\mathbf{h}}$, the spatial average of $\mathbf{z}(\mathbf{x})$ over its 2×2 unit cell. An arbitrary microstate can thus be divided into a set of domains of symmetry-related ideal states, with each domain considered to have a uniform value of $\bar{\mathbf{h}}$. This is the intermediate step in the coarse-graining process, where we are already treating \mathbf{x} as a continuous variable, but $\bar{\mathbf{h}}$ takes on discrete values. In the final step of coarse-graining, we replace $\bar{\mathbf{h}}$ by $\mathbf{h}(\mathbf{x})$ which takes on a continuum of values.

There is a finite number of ideal states, but the values of \mathbf{z} are unbounded; for each allowed $\bar{\mathbf{h}}$ value there is unique ideal state, but for a given ideal state the possible $\bar{\mathbf{h}}$ value is only fixed modulo a Bravais lattice called the “repeat lattice”. Thus the pattern of dimers near any given site is a function of $\bar{\mathbf{h}}$, and hence any local operator $O(\mathbf{x})$ can be expressed as a function $\tilde{O}(\bar{\mathbf{h}})$; furthermore $\tilde{O}(\bar{\mathbf{h}})$ must have the periodicity of the repeat lattice; Thus it can be written as a Fourier sum of terms of form $\exp(i\mathbf{G}^\perp \cdot \mathbf{h}(\mathbf{x}))$ where \mathbf{G}^\perp are reciprocal lattice vectors of the repeat lattice.

The possible values of $\bar{\mathbf{h}}$ in height space constitute the “ideal-state graph”. The fact that the local configuration is more likely to be near an “ideal state” than far from one, is expressed by an additional term

* Note that no microstate has $\mathbf{z}(\mathbf{x}) = \text{constant}$, as will be clear from the form of the height maps, e.g. (2.11) or (2.14-2.15).

$V(\mathbf{h})$ which should be added to the free energy density (2.1). This $V(\mathbf{h})$ can be called a “locking term” since if $V(\mathbf{h})$ were strong enough, it would force the system into long-range order in one of the ideal states. Just like the local operators mentioned above, $V(\mathbf{h})$ has the periodicity of the ideal-state graph, and it too can be labeled by a reciprocal lattice vector of the repeat lattice, \mathbf{G}_{lock} . Standard Kosterlitz-Thouless theory [4] predicts that $V(\mathbf{h})$ becomes relevant in the renormalization-group sense when

$$\eta(\mathbf{G}_{lock}) < 4, \quad (2.10)$$

At that point the height component ought to become smooth (a roughening or “locking” transition). Notice that if the heights are in a “smooth” phase, then the reasoning in Sec. 2.1 implies that the correlations decay to a fixed nonzero value, i.e. that the spin model has long-range order.

2.3 Height mappings for two-color dimer models

In general height mappings, one defines a “microscopic”, discrete-valued height function $\mathbf{z}(\mathbf{x})$ such that the step in $\mathbf{z}(\mathbf{x})$ between adjacent sites is a function of the adjacent spins (or, in this case, dimers). The height representations for two-color models are built in an obvious fashion from those of the simple dimer model.

2.3.1 Review of simple dimer model

We define heights $z(\mathbf{x})$ on the *dual* lattice, i.e. in the centers of each plaquette. We take the standard orientation of every edge pointing from the even to the odd vertex. Say that \mathbf{x} and \mathbf{x}' are neighboring plaquette centers, such that the edge between them is oriented left to right (when looking from \mathbf{x} to \mathbf{x}'); then define the height difference to be

$$z(\mathbf{x}') - z(\mathbf{x}) = +1(-3) \text{ if there is no dimer (is a dimer)} \quad (2.11)$$

on the edge between \mathbf{x} and \mathbf{x}' . Traversing the four plaquette centers surrounding any vertex, the total change in $z(\mathbf{x})$ is $1 + 1 + 1 - 3 = 0$, since every vertex of the original lattice has exactly one dimer emanating from it. Thus $z(\mathbf{x})$ is well-defined everywhere, *provided the dimer covering is complete*. The $\{z(\mathbf{x})\}$ values are indicated in Fig. 1(a).

It should be noted that the triangular Ising antiferromagnet ground states are (essentially) equivalent to the dimer coverings of the honeycomb lattice (each violated bond corresponds to a dimer) so the construction of $z(\mathbf{x})$ here is closely analogous to that of [5], and indeed the square and honeycomb dimer coverings have the same critical exponents [15]. The height map (2.11) for the square lattice case was, in fact, discovered several times in the context of quantum dimer models and nearest-neighbor valence-bond ground states of $s = 1/2$ antiferromagnets [17]; however, it has never been applied to derive exponents in the spirit of Blöte, Hilhorst, and Nienhuis [5].

2.3.2 Height map of the dimer-loop model

Clearly, we can construct heights for the two-color models by letting $\mathbf{z} = (z_B, z_W)$ where z_B and z_W are the height configurations of the black and white dimer configurations, constructed by the rule given in (2.11).

Let’s define the even combination of heights

$$z_1 \equiv \frac{1}{2}(z_B + z_W) \quad (2.12)$$

and the odd combination of heights

$$z_2 = \frac{1}{4}(-z_B + z_W) \quad (2.13)$$

Under the exchange black \leftrightarrow white, $(z_1, z_2) \rightarrow (z_1, -z_2)$.

By inserting (2.12) and (2.13) into (2.11), we can write the dimer-loop height rule in components. When the edge between \mathbf{x} and \mathbf{x}' is oriented as in (2.11),

$$z_1(\mathbf{x}') - z_1(\mathbf{x}) = +1(-1), \quad \text{if there is no dimer (is a dimer)} \quad (2.14)$$

on that edge, and

$$z_2(\mathbf{x}') - z_2(\mathbf{x}) = 0(+1, -1) \quad \text{if there is no dimer (black dimer, white dimer)} \quad (2.15)$$

on the edge.

As already mentioned in Sec. 1.1, if we do not distinguish black from white, this model reduces to the fully-packed loop (FPL) model with loop fugacity $n = 2$. The FPL model for general fugacities admits the same configurations, but with different weights. Any FPL configuration can be mapped 1-to-1 to a configuration of the six-vertex (or “ice”) model:* a bond receives an ice-arrow pointing from the even to the odd vertex, if that bond is occupied by loop segments, and pointing oppositely if the bond is vacant.

The six-vertex model has a well-known height mapping, indeed its height configurations $\{z_1(\mathbf{x})\}$ are simply the microstates of the body-centered solid-on-solid (BCSOS) model [18]. The $\{z_1(\mathbf{x})\}$ sit on the dual lattice and are defined by $z_1(\mathbf{x}') - z_1(\mathbf{x}) = +1(-1)$, according to whether the ice-arrow (viewed looking from \mathbf{x} to \mathbf{x}') points rightwards (leftwards) along the edge between \mathbf{x} and \mathbf{x}' . It can easily be checked that the z_1 configuration defined in (2.14) for the dimer-loop model is identical to the z_1 configuration defined definted by mapping to the FPL and then to the six-vertex model, followed by the six-vertex height rule. (See Fig. 1).

The component z_2 has its own simple interpretation as an SOS model. The loops are simply *contours* of equal height z_2 . If one switched the colors white \leftrightarrow black within one loop, then a step up would be turned into a step down. We could view the rule for $\{z_2(\mathbf{x})\}$ as a constrained SOS model: besides the standard restriction that $|z_2(\mathbf{x}') - z_2(\mathbf{x})| \leq 1$, we also require that every block of four plaquettes must include exactly two pairs of neighboring plaquettes on which $z_2(\mathbf{x}') = z_2(\mathbf{x})$. It is amusing that this SOS model, which would appear to be described by only one height variable, is one-to-one equivalent to the original two-color dimer-loop model and thus contains $z_1(\mathbf{x})$ as a second, hidden height variable.

2.3.3. Height map of the noncrossing-dimer model

To define the heights for both colors of dimer in the noncrossing-dimer model, we arbitrarily define the dual lattice site at $\mathbf{x} + (\frac{1}{2}, \frac{1}{2})$ to have the same parity as the original lattice site at \mathbf{x} . Then we construct height configurations $z_B(\mathbf{x})$ and $z_W(\mathbf{x})$ as before. However, in this model the $\{z_B(\mathbf{x})\}$ live on the original lattice while the $\{z_W(\mathbf{x})\}$ live on the dual lattice, so we cannot at this point define even and odd combinations like (2.12)-(2.13); we shall do so later on, at the coarse-grained stage (see Sec. 2.4).

2.3.4 Ideal states of two-color dimer models

The proposed ideal states for the models in this paper are shown in Fig. 3; they all have 2×2 unit cells. The black or white dimer parts of these two-color ideal states are just ideal states of the simple dimer model. It is straightforward to identify ideal states for the simple dimer and noncrossing-dimer models, but it is not so clear whether Fig. 3(b) or Fig. 3(c) is the best choice in the case of the dimer-loop model. We prefer Fig. 3(b) as it has a smaller variance of the z_1 component; indeed the $z_1(\mathbf{x})$ pattern here is the same as the ideal state of the BCSOS model. On the other hand, the alternative Fig. 3(c) does have a smaller variance of the z_2 component, which is found to be in a “smooth” phase as will be elaborated in Sec. 4

Fig. 1(a) illustrates that real configurations can indeed be broken into “ideal state” domains. Note how all the sites with height “1”, and most of those with height “0” or “2”, are unchanged from a certain ideal state; this is not surprising since such a small system has no room for a large height fluctuation. On the other hand, the local patterns *appear* different from those in an ideal state, in that one rarely finds more than two parallel dimers in a row.

* A six-vertex configuration means a pattern of arrows on the dual lattice such that two ice-arrows are incoming and two are outgoing at every vertex.

Fig. 4 shows the ideal-state graphs for these models. For the case of the simple dimer covering, the $\bar{\mathbf{h}}$ values differ by ± 1 between ideal states, and the repeat lattice constant is 4 (corresponding to the four symmetry-related ideal states). It turns out that the two-color ideal states are made from combinations of the simple-dimer ideal states, but not every combination is ideal or is optimal. For the dimer-loop case, Fig. 4(b), each black dimer ideal state can be combined with only one white dimer ideal state so there are only 4 ideal states. For the noncrossing-dimer case, Fig. 4(d), simple-dimer states can be combined only if both colors of dimers are oriented the same way, so there are 8 ideal states.

2.4 Elastic theory

Next we will work out the allowed symmetry form of the gradient-squared elastic free energy density $f(\nabla\mathbf{h})$. It is quite possible that a 2-dimensional height space would have only one elastic constant (as for the honeycomb two-coloring [6,8]). However, each two-color dimer model here turns out to have two distinct elastic constants.

We proceed in the spirit of Landau theory, by first identifying the transformations of $\{\mathbf{z}(\mathbf{x})\}$ which are induced by a given lattice symmetry operation. Next we identify the coarse-grained version of this symmetry operation, and finally we require that $f(\nabla\mathbf{h})$ be invariant under this symmetry. The elastic theory will be related to critical exponents in Sec. 2.5.

2.4.1 Simple dimer model.

The microscopic transformations are

(i). $x_1 \rightarrow x_1 + 1$ induces $z(\mathbf{x}) \rightarrow -z(\mathbf{x})$ (because our standard orientation of edges alternates between even and odd)

(ii). $x_1 \rightarrow -x_1$ (mirror line through a row of lattice points) induces $z(\mathbf{x}) \rightarrow -z(\mathbf{x})$, and of course $\nabla_1 \rightarrow -\nabla_1$ (we take $\nabla_i \equiv \partial/\partial x_i$). On the other hand, a mirror line through a row of plaquette centers is represented by $x_1 \rightarrow 1 - x_1$ and induces $z(\mathbf{x}) \rightarrow -z(\mathbf{x})$.

(iii). A 4-fold rotation about a vertex induces $z(\mathbf{x}) \rightarrow -z(\mathbf{x})$, $\nabla_1 \rightarrow \nabla_2$, $\nabla_2 \rightarrow -\nabla_1$. On the other hand, a 4-fold rotation about the center of a plaquette induces $z(\mathbf{x}) \rightarrow z(\mathbf{x})$.

Now we consider all possible terms bilinear in gradients of $h(\mathbf{x})$. By (iii) $\nabla_1 h \nabla_2 h \rightarrow -\nabla_1 h \nabla_2 h$ under a symmetry, so this term must have zero coefficient in the free energy. Also $(\nabla_1 h)^2 \rightarrow (\nabla_2 h)^2$, so that those two terms must have equal coefficients. Thus the generic form is

$$f(\nabla h) = \frac{1}{2}K[(\nabla_1 h)^2 + (\nabla_2 h)^2] \quad (2.16)$$

2.4.2 Dimer-loop model

In the two-color dimer models, the above reasoning still holds for all terms which depend purely on h_W or on h_B (the coarse-grained z_W and z_B components), thus we only need to check the h_B - h_W cross-terms.

In the dimer-loop model, the reflection symmetry (ii) transforms $\nabla_1 h_B \nabla_2 h_W \rightarrow -\nabla_1 h_B \nabla_2 h_W$, thus such terms must be absent in $f(\nabla\mathbf{h})$. On the other hand, no symmetry excludes the terms $\nabla_1 h_B \nabla_1 h_W$ and $\nabla_2 h_B \nabla_2 h_W$, and the 4-fold rotation symmetry merely demands that their coefficients be equal. After diagonalizing the quadratic form in $\nabla\mathbf{h}$ we obtain

$$f(\nabla\mathbf{h}) = \frac{1}{2}K_1|\nabla h_1|^2 + \frac{1}{2}K_2|\nabla h_2|^2 \quad (2.17)$$

where

$$(h_1, h_2) = \left(\frac{1}{2}(h_B + h_W), \frac{1}{4}(h_B - h_W)\right) \quad (2.18)$$

is the coarse-grained version of (z_1, z_2) defined by (2.12) and (2.13).

We might have guessed the form (2.17) from a glance at the ideal-state graph (Fig. 4(b)), which shows that the h_1 and h_2 directions are not equivalent by any symmetry. Fig. 4(b) also suggests that the stiffness

should be greater for the $(1, -1)$ projection of height space than for the $(1, 1)$ projection, since fluctuations in the former direction must pass through several steps to get from one favorable (ideal) state to the next one. After the above changes of variables, this expectation translates to the inequality $K_2 \geq 4K_1$.

2.4.3 Noncrossing-dimer model

This case is subtler. A mirror line that passes through a lattice point in the *black* lattice runs through *plaquette* centers in the dual *white* lattice, hence a reflection induces e.g. $\nabla_1 \rightarrow -\nabla_1$, $h_B \rightarrow h_B$, $h_W \rightarrow -h_W$; the analogous thing happens with the 4-fold rotation. For this case, the cross-terms $\nabla_1 h_B \nabla_1 h_W$ and $\nabla_2 h_B \nabla_2 h_W$, are excluded, while $\nabla_1 h_B \nabla_2 h_W$ and $\nabla_1 h_B \nabla_2 h_W$ are allowed, with the 4-fold symmetry demanding that their coefficients be equal.

We adopt height-space coordinates rotated by 45° ,

$$h_1 \equiv \frac{1}{\sqrt{2}}(h_B + h_W), \quad h_2 \equiv \frac{1}{\sqrt{2}}(-h_B + h_W) \quad (2.19)$$

– as in the dimer-loop model, except that here h_1 and h_2 are related by a symmetry. To represent the elasticity in the simplest form, we must also rotate *real* space by 45° defining coordinates \mathbf{y} :

$$y_1 \equiv \frac{1}{\sqrt{2}}(x_1 + x_2), \quad y_2 \equiv \frac{1}{\sqrt{2}}(-x_1 + x_2). \quad (2.20)$$

and the wavevector \mathbf{q} is defined by the corresponding rotation on \mathbf{p} . Under these changes of variables, the elastic terms noted in the first paragraph yield as the generic form,

$$f(\nabla \mathbf{h}) = \frac{1}{2}K_+ (|\frac{\partial}{\partial y_1} h_1|^2 + |\frac{\partial}{\partial y_2} h_2|^2) + \frac{1}{2}K_- (|\frac{\partial}{\partial y_1} h_2|^2 + |\frac{\partial}{\partial y_2} h_1|^2) \quad (2.21)$$

with two independent elastic constants K_+ and K_- .

A consequence of (2.21) plus equipartition is that the generalization of (2.3) reads

$$\langle |h_1(\mathbf{p})|^2 \rangle = (K_+ q_1^2 + K_- q_2^2)^{-1} \quad (2.22)$$

with $\langle |h_2(\mathbf{p})|^2 \rangle$ defined by exchanging $1 \leftrightarrow 2$ in (2.22).

There is a simple argument that $K_+ > K_-$. It can be checked that, with our even/odd conventions, the contribution to $\partial h_B / \partial x_1$ made by a black dimer on a vertical bond has the same sign as the contribution to $\partial h_W / \partial x_2$ that a white dimer on the horizontal crossing bond would have made. The exclusion between these possibilities has the effect of a positive term in the free energy proportional to $(\partial h_B / \partial x_1)(\partial h_W / \partial x_2)$; a similar argument works for $x_1 \leftrightarrow x_2$. After we carry out the above changes of variable, we find that $K_+ - K_-$ in (2.21) is proportional to the positive coefficient of those terms.

2.5 Critical Exponents for two-color dimer models

We can now calculate the correlation function exponents by the path sketched in Sec. 2.1, but adapting to $d^\perp > 1$ in two ways:

(i) the elasticity has a more complicated form than eq. (2.1), when there is more than one elastic constant.

(ii) the spin operators are now represented by

$$\exp(i\mathbf{G}^\perp \cdot \mathbf{h}(\mathbf{x})) \quad (2.23)$$

where \mathbf{G}^\perp is a vector of the reciprocal lattice of the “repeat lattice” in the height space;* similarly, a defect Burgers vector \mathbf{b} must be a vector of the repeat lattice.

* The dominant wavevector \mathbf{G}^\perp for a given operator can be deduced easily with the aid of the “ideal states” graph. We have omitted this detail in the present paper; the method is explained in Ref. [10].

The previously known example of a two-dimensional height space was the 3-coloring of the honeycomb lattice. That model is (essentially) equivalent to the 3-state-Potts antiferromagnetic ground states on the Kagome lattice [6], the 4-state-Potts antiferromagnetic ground states on the triangular lattice [3], and the “fully-packed loop (FPL) model” on the honeycomb lattice [7,8]. Given one previously known exponent of this model, Huse and Rutenberg used the arguments reproduced in Sec. 2.1 to find the correlation function exponent of the Kagomé 3-state-Potts model [6] (later additional exponents in the FPL model were calculated in the same fashion [8]).

2.5.1 Dimer-loop model

In this model, dimer-dimer correlations which do not depend on the dimer color are governed by $\mathbf{G}^\perp = (G_1^\perp, G_2^\perp) = (2\pi/2, 0)$; those that treat black and white dimers as having opposite signs are governed by $\mathbf{G}^\perp = (2\pi/4, 2\pi/2)$. The exponents are given by

$$\eta(\mathbf{G}^\perp) = \frac{1}{2\pi K_1} |G_1^\perp|^2 + \frac{1}{2\pi K_2} |G_2^\perp|^2 \quad (2.24)$$

A defect of type $\mathbf{b} = (b_1, b_2) = (2, 1)$ corresponds to an endpoint of a loop, while $\mathbf{b} = (0, 1)$ corresponds to having two successive segments of the same color in a loop. The exponents are given by

$$\eta_v(\mathbf{b}) = \frac{K_q}{2\pi} |b_1|^2 + \frac{K_2}{2\pi} |b_2|^2 \quad (2.25)$$

2.5.2 Noncrossing-dimer model

In this case, there are nontrivial modifications in the derivation on account of the anisotropic elasticity. The height correlation function is $C_k(\mathbf{x}) = \langle [h_k(\mathbf{x}) - h_k(0)]^2 \rangle$ (for $k = 1, 2$). Substituting from (2.22), and rescaling the coordinates

$$(q'_1, q'_2) \equiv (\lambda q_1, \lambda^{-1} q_2), \quad (y'_1, y'_2) \equiv (\lambda^{-1} y_1, \lambda y_2) \quad (2.26)$$

(where $\lambda \equiv (K_+/K_-)^{1/4}$), we obtain

$$C_1(\mathbf{x}) = \int \frac{dq'_1 dq'_2}{(2\pi)^2} \frac{2(1 - \cos(\mathbf{q}' \cdot \mathbf{y}'))}{\bar{K} |\mathbf{q}'|^2} = \text{const} + \frac{1}{\bar{K}\pi} \ln |\mathbf{y}'|, \quad (2.27)$$

where $\bar{K} \equiv (K_+ K_-)^{1/2}$. ($C_2(\mathbf{x})$ is also given by (2.27) but with $\lambda \leftrightarrow \lambda^{-1}$ in (2.26)). Recall that in all these formulas, \mathbf{y}' is rewriting of \mathbf{x} through (2.20); in particular if we write $\mathbf{x} = |\mathbf{x}|(\cos \theta, \sin \theta)$, then $|\mathbf{y}'| = |\mathbf{x}| f(\theta, \lambda)^{1/2}$ where

$$f(\theta) = \lambda^2 \cos^2(\theta - \pi/4) + \lambda^{-2} \sin^2(\theta - \pi/4). \quad (2.28)$$

Thus if an operator is written in the form $O(\mathbf{x}) \sim \exp(i\mathbf{G}^\perp \cdot \mathbf{h}(\mathbf{x}))$, it follows as usual that

$$\langle O(\mathbf{x})O(0) \rangle = \exp(-\frac{1}{2} \langle [\mathbf{G}^\perp \cdot (\mathbf{h}(\mathbf{x}) - \mathbf{h}(0))]^2 \rangle). \quad (2.29)$$

This can be written

$$\langle O(\mathbf{x})O(0) \rangle = \exp(-\frac{1}{2} [(G_1^\perp)^2 C_1(\mathbf{x}) + (G_2^\perp)^2 C_2(\mathbf{x})])$$

where \mathbf{G}^\perp has been resolved into components in the (h_1, h_2) basis. Inserting the logarithm (2.27) into the exponential (2.29), we finally get

$$\langle O(\mathbf{x})O(0) \rangle \sim |\mathbf{x}|^{-\eta(\mathbf{G}^\perp)} f(\theta)^{\eta_1} f(\theta - \pi/2)^{\eta_2} \quad (2.30)$$

where

$$\eta_k \equiv \frac{1}{2\pi \bar{K}} (G_k^\perp)^2$$

for $k = 1, 2$, and

$$\eta \equiv \eta_1 + \eta_2 = \frac{1}{2\pi\overline{K}}|\mathbf{G}^\perp|^2 \quad (2.31)$$

Thus, the exponents $\eta(\mathbf{G}^\perp)$ for the noncrossing-dimer model, have just the form that would follow from an isotropic effective elasticity with one elastic constant \overline{K} . However, the decay of correlations is not isotropic, as in other known cases, but has the anisotropy factors $f(\cdot)$ displayed in (2.30).

The defect-defect correlation function corresponding to a Burgers vector \mathbf{b} would have an exponent

$$\eta_v(\mathbf{b}) = (2\pi)^{-1}\overline{K}|\mathbf{b}|^2 \quad (2.32)$$

but with exotic anisotropy factors analogous to those in (2.30).

3. MONTE CARLO SIMULATIONS AND RESULTS

Monte Carlo simulations were performed for the dimer-loop and noncrossing dimer models in square lattices with periodic boundary conditions. Besides the new models introduced in this paper, we have also simulated two exactly solved models as checks (both for debugging of our simulation codes, and to test how much accuracy may be obtained from this way of analyzing the results.) (i) Since both z_1 and z_2 have configurations like those of a simple SOS model, we chose to simulate the BCSOS model. (ii) We also simulated the simple dimer model.

In this section, we present in turn the update moves, the simulation protocol, and the numerical results.

3.1 Update moves

In some “height” models – e.g. the square lattice four-coloring model [10] or the constrained Potts antiferromagnet [12] – a nonlocal cluster or loop update move is required. In each of the two-color dimer models, however, a local update move, based on the rearrangements shown in Fig. 2, was adequate. A “pass” thus consisted of visiting each site once (in random order), testing whether the site could be rearranged, and if so changing it. These update rules satisfy detailed balance for the ensemble in which each microstate receives equal statistical weight.

There is an important technicality associated with the question of ergodicity, in the presence of our periodic boundary conditions. Let $\Delta_1\mathbf{z} = \mathbf{z}(L, 0) - \mathbf{z}(0, 0)$ and $\Delta_2\mathbf{z} = \mathbf{z}(0, L) - \mathbf{z}(0, 0)$. These are Burgers vectors associated with the topologically nontrivial loops on the torus, and so they must belong to the repeat lattice. Then $\Delta_1\mathbf{z}$ and $\Delta_2\mathbf{z}$ are conserved under all *local* update moves, including ours. The average of the height gradient $\nabla_i\mathbf{h}$ is $\Delta_i\mathbf{h}/L$, thus we are sampling an ensemble with a fixed average slope. (Our moves *do* access all the microstates with a given $(\Delta_1\mathbf{h}, \Delta_2\mathbf{h})$.)

We have just the same problem as if we were trying to study the thermodynamics of an Ising model in zero field, but using an update which conserves spin. If we are in a paramagnetic state, we know that in the thermodynamic limit the magnetization is zero, and so we obtain the right results if we adopt initial conditions with zero total spin; however, we would have problems below the symmetry-breaking temperature.

Here, we believe that the thermodynamic state has zero mean height slope (whether the heights are rough or smooth). Thus we require choose initial conditions with $\Delta_i\mathbf{h} \equiv 0$. (This is possible when L is even.) This also means that $\mathbf{z}(\mathbf{x})$ is single-valued and we can perform a Fourier transform without needing to subtract off the average slope $\nabla\mathbf{h}$.

The update rule of the simple dimer model is shown in Fig. 2(a). Since each color of dimer must maintain a complete covering, every update move of the two-color dimer models is built from the update in Fig. 2(a): either one color is updated (as in Fig. 2(b)), or both colors are updated at the same time (as in Fig. 2(c) and 2(d)).

Given a generic free energy of form (2.1), standard arguments [19] would suggest a coarse-grained description of the Monte Carlo dynamics would be

$$dh_{\mathbf{q}}(t)/dt = \zeta_{\mathbf{q}} - \Gamma K|\mathbf{q}|^2 h_{\mathbf{q}}(t) \quad (3.1)$$

where Γ is a kinetic coefficient and the random noise satisfies $\langle \zeta_{\mathbf{q}}(t)\zeta_{\mathbf{q}'}(t') \rangle = 2\Gamma\delta_{\mathbf{q},\mathbf{q}'}\delta(t-t')$. Thus the relaxation time is expected to be wavevector-dependent as $\tau(\mathbf{q}) \sim |\mathbf{q}|^{-2}$ [11].

3.1.1 Dimer-loop model

The configurations were represented in the machine as configurations of z_2 . As noted above in Sec. 2.3.2, the values of z_1 may be (and were) reconstructed uniquely from those of z_2 .

The update moves we used correspond to the two rearrangements illustrated in Fig. 2(b,c) in terms of z_2 (or the moves related to them by symmetry). Both rules are necessary in order to access all the microstates. Notice that the move in Fig. 2(c) has no effect on the z_1 coordinate.

For our simulations of the BCSOS model, the update move looks the same as Fig. 2(c).

3.1.2 Non-crossing dimer model

The configurations were represented as patterns of (z_B, z_W) . In order to ensure detailed balance for the update of the noncrossing-dimer model, we choose at random a plaquette of the black-dimer lattice and one of the four plaquettes of the dual (white-dimer) lattice that overlap the first plaquette; we check whether a rearrangement involving these plaquettes is possible, and if so we carry it out.

Including the move shown in Fig. 2(e) would have speeded up the simulation, but we did *not* implement it. We think that the Fig. 2(d) move, by itself, in time can access every configuration that the Fig. 2(e) move can access.

A somewhat worrisome aspect of our update move is that it is not fully ergodic. Namely, if we let M_B (M_W) be the number of black(white) dimers oriented in the x direction, then $M_B - M_W$ is *conserved* (by either of the possible update moves in Fig. 2). However, we do not think this invalidates the results. The thermodynamic limit is surely dominated by $(M_B - M_W)/N = 0$, and our simulations have $M_B - M_W = 0$ (or very nearly zero, in the “roof” initial condition). Thus our ensemble, restricted by the conservation law, is related to the full one much as a microcanonical ensemble is related to a canonical one; such differences are usually irrelevant in the thermodynamic limit.

A more serious criticism is that there exist certain configurations, (having zero mean height gradient) which contain *no* examples of the updatable configuration, Fig. 2(d). A portion of a periodic pattern of this sort is shown in Fig. 2(f). This means that we are in fact simulating a modified ensemble, in which such microstates are not included. However, such states are a vanishing fraction of the total ensemble, and do not matter in the thermodynamic limit. (If one takes the state in Fig. 2(f), and changes it in just one place, this introduces an example of the Fig. 2(d) pattern; then, starting from that place, it is possible by iteration of the update move to reach the canonical flat state shown in Fig. 3(d).)

3.2 Simulation protocol

One “sweep” consists of one random update per site. At sampling intervals of n_s sweeps, we evaluate the Fourier transform, and accumulate the results in sums of $|\tilde{\mathbf{z}}(\mathbf{p})|^2$, where

$$\tilde{\mathbf{z}}(\mathbf{p}) \equiv \frac{1}{\sqrt{N}} \sum_{\mathbf{x}} e^{i\mathbf{p}\cdot\mathbf{x}} \mathbf{z}(\mathbf{x}) \quad (3.2)$$

(The correlation time for the shortest wavevectors is long enough that sampling at shorter intervals would be redundant.) For both models, $\tilde{\mathbf{z}}(\mathbf{p})$ was evaluated for all \mathbf{p} using the fast-Fourier transform (FFT).

In the case of the noncrossing-dimer model, we did not (and cannot!) define $\mathbf{z}(\mathbf{x})$, as $z_B(\mathbf{x})$ and $z_W(\mathbf{x})$ are defined on different sublattices of $\{\mathbf{x}\}$. To implement to (2.19), we define $\tilde{z}_1(\mathbf{p})$ and $\tilde{z}_2(\mathbf{p})$ by

$$[\pm\tilde{z}_B(\mathbf{p}) + \tilde{z}_W(\mathbf{p})]/\sqrt{2} \quad (3.3)$$

Here $\tilde{z}_W(\mathbf{p})$ is actually computed by taking the FFT of the function $z_W(\mathbf{x} + [1/2, 1/2])$ and multiplying by the $e^{i\mathbf{p}\cdot(1/2,1/2)}$. *

* Notice that, by (3.3), $\tilde{z}_1(\mathbf{p})$ is *not* periodic modulo the Brillouin zone, but only modulo a doubled

Data was typically sampled (taking the FFT) once every 100 sweeps. On an IBM RISC-6000/320 workstation, each dimer-loop run of 1.4×10^6 sweeps on a 64×64 lattice took ~ 150 hours, and each noncrossing-dimer run of 5×10^5 sweeps on a 32×32 lattice took ~ 10 hours. The results reported here are averaged from ~ 10 runs for each model studied. (For the test models, simple dimers and BCSOS, much less computing effort was necessary).

To provide a check on equilibration, two kinds of initial condition were used. † The first is an ideal state, so that the heights are as flat as possible (see Fig. 3(a,b,c) again). All the Fourier components $\tilde{\mathbf{z}}(\mathbf{p})$ are initially zero, except at $\mathbf{p} = (\pi, 0)$, $(0, \pi)$, and (π, π) ; typically $|\tilde{\mathbf{z}}(\mathbf{p})|^2$ grows with time. The second initial condition is a “roof” pattern of heights, which is illustrated in Fig. 3(d) for the case of the simple-dimer model. In this case the excursion of $\mathbf{z}(\mathbf{x})$ from its mean is $O(L)$, much larger than in equilibrium where it is $O(\sqrt{\ln L})$, and farther from equilibrium than the ideal state. If the height gradient of the “roof” runs in the x_1 direction, then $\tilde{\mathbf{z}}(p, 0)$ is initially large and different in magnitude from $\tilde{\mathbf{z}}(0, p)$. With time, the mean-squared $\tilde{\mathbf{z}}(p, 0)$ decreases and mean-squared $\tilde{\mathbf{z}}(0, p)$ increases until they are equal, as required by symmetry. This was our diagnostic that equilibrium was reached in the time allotted. The initial difference between “roof” and “flat” initial conditions is most extreme at the smallest wavevectors, which by (3.1) are the slowest relaxing ones; thus our diagnostic provides a sensitive test whether our run time is adequate. (This is further commented in Sec. 3.3, below).

To test our method to extract elastic constants, we also tested *exactly solved* models with height space dimension $d^\perp = 1$ and with similar height mappings. For the dimer-loop model, the BCSOS model was our test model; for the noncrossing-dimer model, the simple dimer model was the test model.

3.3 Results

Our fitting procedure was to perform a linear-least-squares fit of $\langle\langle |\tilde{\mathbf{z}}_i(\mathbf{p})|^2 \rangle\rangle^{-1}$ to a polynomial in (p_1, p_2) with all quadratic and quartic terms, using data from a disk, roughly $|\mathbf{p}| < 0.15\pi$. (If the quartic correction terms are omitted, the fitted elastic constants have systematic errors of $> 1\%$.)

The data (for selected wavevectors) are shown in Figs. 5-8 for the four models (BSCOS, simple dimers, dimer-loop, and noncrossing-dimer). Notice that Figs. 5-8 do not include all the data used for our fits: for clarity, we have shown only one-dimensional cuts through reciprocal space. However, where two values ought to be identical according to the symmetries of the model, we have plotted both of them. We premultiply by $P(\mathbf{p})^2 \equiv 2(2 - \cos p_x - \cos p_y)$, a Brillouin-zone adapted version of $|\mathbf{p}|^2$, so that the plots should asymptote to a constant as $\mathbf{p} \rightarrow 0$, if they follow the expected behavior for a rough interface.*

In the non-crossing dimer plot, one of the data points for the shortest wavevector ($|\mathbf{p}| = 2\pi/32$) is too low (compared to the line through the other data points), while the data points for the other symmetry-related wavevectors of the same length are about right. This is due solely to the Fourier component $\tilde{z}_1(\pi/16, 0)$ being spuriously large (by a factor of 1.5) in the data sets using the “roof” initial condition. That shows that the equilibration time we allowed was, in fact, *not* longer than the longest relaxation time (however, all other wavevectors appear to be equilibrated). Presumably the same explanation applies to the similar (but smaller) discrepancies visible in some of the other plots.

The elastic constants extracted from the best fits are shown in Table I. The error which we choose to quote is taken as twice the statistical error, to allow for systematic errors. (The statistical errors were calculated from the variance of the fitted elastic constants from at least four independent runs of the same model.) For the new models, we indicate conjectures (marked by “?” in the Tables), assuming that the stiffnesses are simple rational multiples of π (which would be the condition for having rational critical exponents).

Table II shows the predicted correlation exponents when the (known or conjectured) exact stiffnesses

zone, so e.g., $\tilde{z}_1(\pi, p_2) \neq \tilde{z}_2(-\pi, p_2)$. The correct relationship is that $\tilde{z}_1(\mathbf{p} + (2\pi, 0)) = \tilde{z}_2(\mathbf{p})$, and similarly $\tilde{z}_2(\mathbf{p} + (0, 2\pi)) = \tilde{z}_1(\mathbf{p})$.

† The data averages reported include the entire simulation, so the run time should be much larger than the equilibration time in order to minimize systematic errors due to the initial configurations.

* In the case of the simple dimer model, replacing $|\mathbf{p}|^2$ by $P(\mathbf{p})^2$ made a visible difference: most of the variation of $|\mathbf{p}|^2 \langle |\tilde{\mathbf{z}}(\mathbf{p})|^2 \rangle$ with \mathbf{p} was cancelled.

in Table I are inserted into the theoretical formulas (2.8) and (2.9) (or their generalizations (2.24), (2.25), (2.31), and (2.32) in Sec. 2.5). Recall that $\eta(\mathbf{G}^\perp)$ are exponents for local operators, e.g. the dimer-dimer correlation, while $\eta(\mathbf{b})$ are for defect operators.

4. DISCUSSION OF RESULTS

In this section, we review our expectations for a general height model, in the light of Sec. 2.1, and then try to make sense of the prominent features of the results.

4.1 General expectations for behavior of $\langle |\tilde{z}(\mathbf{p})|^2 \rangle$

The prime expectation is a consequence of coarse-graining (Sec. 2.1). Near $\mathbf{p} = 0$, i.e. averaged over long wavelengths, $\mathbf{z}(\mathbf{p}) \approx \mathbf{h}(\mathbf{p})$. Thus if the height field is in a “rough” phase, eq. (2.3) implies

$$\langle |\tilde{z}(\mathbf{p})|^2 \rangle^{-1} \sim K |\mathbf{p}|^2 \quad (4.1)$$

in a one-dimensional height model; for $d^\perp = 2$, (4.1) has its obvious generalizations in terms of the elastic theory of Sec. 2.4.

On the other hand, our usual picture of a “smooth” phase is that the system is in an ideal state on the majority of the sites. The fluctuations in equilibrium consist of individual sites, or very small domains, on which the heights deviate from the ideal state. Since these fluctuations are local and do not overlap, they ought to be independent. Hence their Fourier transform should have a white-noise spectrum,

$$\langle |\tilde{z}(\mathbf{p})|^2 \rangle \sim \text{const} \quad (4.2)$$

as $\mathbf{p} \rightarrow \mathbf{0}$.

It should be noted that the general definition of a “smooth” phase in an SOS model is that the net height variance

$$W^2 \equiv \langle \mathbf{z}(\mathbf{x})^2 \rangle - \langle \mathbf{z}(\mathbf{x}) \rangle^2 \quad (4.3)$$

is finite in the thermodynamic limit. Thus, smoothness means that the system undergoes a symmetry-breaking in which a particular mean height is picked out with long-ranged order. Writing the height variance as

$$W^2 = \sum_{\mathbf{p} \neq 0} \langle |\tilde{z}(\mathbf{p})|^2 \rangle. \quad (4.4)$$

it can be seen that on insertion into (4.4), the smooth behavior (4.2) indeed gives a convergent sum while the rough behavior (4.1) gives the well-known logarithmic divergence,

$$W^2 = \text{const} + \frac{1}{2\pi K} \ln L \quad (4.5)$$

since the sum (4.4) is cut off at the smallest \mathbf{p} which is of order $1/L$.

A generic feature in height model data is the presence of zone-boundary singularities of $\langle |\mathbf{z}(\mathbf{p})|^2 \rangle$ for \mathbf{p} near $\mathbf{Q}^{(1)} = (\pi, 0)$ and $\mathbf{Q}^{(2)} = (\pi, \pi)$. This is a consequence of the fact that \mathbf{z} is not uniform even in an ideal state; rather $\mathbf{z} - \bar{\mathbf{h}}$ is modulated at wavevectors $\mathbf{Q}^{(i)}$. The amplitude of modulation itself is a periodic function of the heights, thus it is an operator of form $\hat{O}(\mathbf{h}) \sim \exp(i\mathbf{G}^{(i)} \cdot \mathbf{h})$, implying power-law correlations as explained in Sec. 1. Following this through (Ref. [10] gives more details for the case of the 4-coloring model), we predict

$$\langle \tilde{z}(\mathbf{p})|^2 \rangle \sim |\mathbf{p} - \mathbf{Q}^{(i)}|^{-(2-\eta^{(i)})} \quad (4.6)$$

where $\eta^{(i)} = \eta(\mathbf{G}^{(i)})$.

In the case of the simple dimer model, examination of the modulations gives $G^{(1)} = 2\pi/4$ and $G^{(2)} = 2\pi/2$, implying (see Table II) that $\eta^{(1)} = 1/2$ and $\eta^{(2)} = 2$. Examination of our data from this model shows

that the fluctuations indeed have a small peak at $(\pi, 0)$ and are constant near (π, π) . Such zone-boundary peaks have also been seen in simulations of other height models [10,11].

In the discussion of each model, we will check the plausibility of the behavior and numerical value of the stiffness constant by considering the models as modifications of exactly solved models. In particular, we may define generalized “ghost” versions of the two-color dimer models by discarding the hard-core exclusion between black and white dimers. Instead we might include a weight factor e^{-u} in the partition function for each such violation. Thus the $u = \infty$ case is the models we simulated, and the $u = 0$ case is the noninteracting limit consisting of two copies of the simple dimer model.

Presumably the stiffness constants are monotonic functions of u . Since the exclusion rules still permit flat “ideal” states, but permit fewer ways of fluctuating away from them, we anticipate that the stiffness constants increase as we turn on u . If so, then the elastic constants for the noninteracting cases, which may be found trivially by applying the changes of variables (2.17) and (2.18), supply a lower bound on the expected results.

4.2 Dimer-loop model

The dimer-loop model data could be fit to $\langle |\tilde{z}_1(\mathbf{p})|^2 \rangle \sim 1/(K_1|\mathbf{p}|^2)$ as expected for the “rough” behavior (4.1). However, it is evident from Fig. 7(a) that (after excluding the smallest \mathbf{p} value, see Sec. 3.3), these data deviate more strongly at small \mathbf{p} in the other models. They might be fit to a different exponent, roughly $\langle |\mathbf{z}_1(\mathbf{p})|^2 \rangle \sim |\mathbf{p}|^{-1.9}$, but this is so close to $|\mathbf{p}|^{-2}$ that the latter seems more plausible. Perhaps the deviation can be blamed on coupling to the anomalous smooth component z_2 (see below). As expected, $\langle |\tilde{z}_1(\mathbf{p})|^2 \rangle$ also shows slight maxima at the zone-boundary points $\mathbf{Q}^{(1)}$ and $\mathbf{Q}^{(2)}$.

However, as is obvious from Fig. 7(b), the second height component has a different behavior:

$$\langle |\tilde{z}_2(\mathbf{p})|^2 \rangle \sim |\mathbf{p}|^{-(2-\eta^{(0)})} \quad (4.7)$$

with $2 - \eta^{(0)} \approx 1$, very roughly. (The apparent exponent varies from ~ 0.6 at the smallest $|\mathbf{p}|$ to ~ 1.2 at larger $|\mathbf{p}|$.) The fact that $\eta^{(0)} > 0$ implies the z_2 component is “smooth” in the sense that its variance, W_2^2 , is finite.

Thus we are led to an approximate picture in which $z_2(\mathbf{x})$ is an ideal state configuration, on which bounded fluctuations are superposed. (It is quite possible to have anomalous power-law correlations, yet have strictly bounded height fluctuations.) Indeed, examination of Fig. 1 (b) shows that z_2 deviates at most ± 2 from the ideal state; furthermore the mean z_2 is 7.51, compared with 7.5 in the ideal state. The same picture predicts that $\langle |\tilde{z}_2|^2 \rangle$ has a zone-boundary peak at $\mathbf{Q}_1 = (\pi, 0)$ approximating a δ -function, which is indeed seen in the data.

4.1.1 The anomalous smoothness of z_2

The smoothness of z_2 is anomalous in that (4.7) is quite different from (4.2), the behavior for a generic “smooth” phase. The probable explanation is that z_2 deviations experience a power-law effective coupling, mediated by the critical z_1 fluctuations.

As an approximation, let us take an ansatz that z_2 is constrained to take on only two values, say 0 and 1. In the partially coarse-grained picture (see Sec. 2.2), the system consists entirely of domains with $h_2 = 1/2$, while h_1 can still take any value $m + 1/2$. However, it can be checked that each domain wall has a net excess $\delta z_2 = \pm 1/4$ per lattice constant in the x_1 or x_2 direction. Let us say $h_1 = m$ along the domain wall separating states with $h_1 = m - 1/2$ and $h_1 = m + 1/2$. It turns out that the sign of the excess is independent e.g. of the wall orientation; it is a function only of m (or h_2) with period 4, taking values in the repeating sequence $1/4, 1/4, -1/4, -1/4$. This can be written

$$\delta z_2 \simeq \frac{1}{2\sqrt{2}} \cos \frac{\pi}{2} (h_2 - \frac{1}{2}). \quad (4.8)$$

Thus we have put the operator δz_2 into the form (2.6) with $\mathbf{G}^\perp = (\pi/2, 0)$. Consequently, using (2.8) and the conjectured exact value of K_1 from Table I, we obtain $\eta^{(0)} = \eta(\mathbf{G}^\perp) \approx 1/2$. (The data (4.7), however, definitely point to a smaller value of $\eta^{(0)}$.)

4.1.2 Comparison to exactly solved models

First let us forget the z_2 component (since it is smooth anyhow) and consider the uncolored FPL model introduced in Sec. 2.2, with stiffness $K_{FPL}(n)$. The $n = 1$ case of the FPL is the equal-weighted six-vertex or “ice” model, which in the height representation is equivalent to the (exactly solved) BCSOS model. Now, increasing the loop fugacity n from 1 favors configurations which have many small loops, and are thus flatter in the height representation. (The state with the maximum number of loops is the one in Fig. 3(c), which also has maximum flatness.) Thus $K_{FPL}(n)$ should increase with n , and indeed Table I shows that $K_1 \equiv K_{FPL}(2)$ is larger than the stiffness of the (equal-weighted) BCSOS model $K = K_{FPL}(1) = \pi/6$.

For an independent comparison to an exactly solved model, consider the “ghost” dimer-loop model, in its noninteracting limit. This has elastic constants $K_1^{(0)} = 2K_0 = \pi/8 \approx 0.3927$ and $K_2^{(0)} = K_0 = \pi/2$. It can be checked, using Fig. 4(b), that the reciprocal lattice vector for locking in the z_2 direction is $\mathbf{G}_{lock}^{(2)} = (0, 2\pi)$ and hence $\eta(\mathbf{G}_{lock}^{(2)}) = 4$: thus the “ghost” model is exactly marginal. Increasing K_2 , by turning on the dimer exclusion u infinitesimally, would reduce $\eta(\mathbf{G}_{lock}^{(2)})$, and consequently by (2.10) h_2 should immediately lock (unroughen).

On the other hand, returning to the FPL representation, it has been observed recently that in loop models, $\eta(\mathbf{G}_{lock})$ is typically marginal, for the height component whose contours form the loops [2]. (Such models include the honeycomb lattice FPL model [7,8], and the 4-coloring model on the square lattice [10].) This criterion would predict a finite value $K_2 = \pi/2$ for the dimer-loop model (presumably K_2 would stay constant for *all* u in the “ghost” model; only K_1 would increase as the dimer exclusion is gradually turned on.) Our data (Fig. 7(b)) clearly exclude this possibility; clearly z_1 is not marginal either, since $\eta(\mathbf{G}_{lock}) = \eta((2\pi, 0)) \approx 8$.

4.3 Noncrossing-dimer model

After converting (2.21) and (2.22) from \mathbf{q} coordinates back to \mathbf{p} coordinates, we obtain

$$\langle |z_1(\mathbf{p})|^2 \rangle^{-1} = \frac{1}{2}(K_+ + K_-)|\mathbf{p}|^2 + \frac{1}{2}(K_+ - K_-)2p_1p_2 \quad (4.9)$$

near $\mathbf{p} = \mathbf{O}$, and the same for $\langle |z_2(\mathbf{p})|^2 \rangle$ except for a change of sign in the second term. The lack of isotropy seen in Fig. 8 is consistent with (4.9).

The difference in Table I between the measured K_+ and our conjectured exact value $\pi/12$ is significant. We have included this conjecture, nevertheless, for two reasons. Firstly, fits using a somewhat larger portion of \mathbf{p} space yielded systematically higher values of the elastic constants, suggesting that our best fit value is still a bit too high; secondly, this conjecture implies a rational value of $(K_+/K_-)^{1/2}$, so that the geometric mean \overline{K} (see Sec. 2.5) can also be a rational multiple of π , which in turn (by (2.31) and (2.32)) implies *rational* critical exponents. Our conjectured value is

$$\overline{K} = \pi/9 \quad (4.10)$$

The data show zone-boundary peaks of $\langle |\tilde{z}(\mathbf{p})|^2 \rangle$ near $\mathbf{Q}^{(1)} = (\pi, 0)$; the existence of peaks suggests that $\eta^{(1)} < 2$, however the data are too crude to estimate the exponent quantitatively. On the other hand, the theory of eq. (4.6) would predict $\eta^{(1)} = \eta(\pi/2, \pi/2) = 9/4$.

Near the zone corner $\mathbf{Q}^{(2)} = (\pi, \pi)$, more complicated behavior is observed. Approaching along the (1,1) direction, the $\langle |\tilde{z}_1(\mathbf{p})|^2 \rangle$ component *vanishes* as $\mathbf{p} \rightarrow \mathbf{Q}^{(2)}$, roughly as $|\mathbf{p} - \mathbf{Q}^{(2)}|^2$; in accord with the symmetry here, $\langle |\tilde{z}_2(\mathbf{p})|^2 \rangle$ behaves the same along the (1,-1) directions. (Approaching $\mathbf{Q}^{(2)}$ along the orthogonal directions, a constant limit is observed, but this is really an independent wavevector; see the footnote in Sec. 3.2).

To understand what is going on at $\mathbf{Q}^{(2)}$, note that $\tilde{z}_1(\mathbf{Q}^{(2)}) = 2(M_B - M_W)$, the excess of dimers of one color in a given orientation. Evidently, the long-wavelength fluctuations of this quantity are divergent. Possibly this behavior is an artifact of the dynamics we used, which (as noted earlier) conserve $M_B - M_W$. But if that is the case, it cannot simply be a memory effect of the initial configuration (since that has

$M_B - M_W \approx 0$). It is equally hard to blame the divergence on random fluctuations which develop during the runs (and then persist because the conservation slows down the dynamics at those wavevectors): the divergent part does not differ from run to run, as would be expected from this explanation. An alternative hypothesis is that the excess $M_B - M_W$ (or, more precisely, the corresponding local density of the excess) functions like a third height variable in the free energy (thus explaining the inverse-square power of the divergence). However, it cannot be a height variable in the usual sense, since the system is not invariant under shifts of the excess. Thus, at present we have no convincing explanation of the divergence at $\mathbf{Q}^{(2)}$.

Comparison to exactly solved models

The noninteracting “ghost” dimer model has $K_+(0) = K_-(0) = K_0 \approx 0.3927$. The value for K_+ in Table II is, as expected, greater than $K_+(0)$, however K_- is *smaller* than $K_-(0)$.

5. CONCLUSIONS

We have defined two new dimer models which have two-dimensional height representations as worked out in Sec. 2.2 and 2.3. (A third new height model presented here is the Ising model mentioned in Sec. 4.2, which was not simulated). By accumulating the mean-squared height fluctuations of each Fourier mode as analyzed from a Monte Carlo simulation, we have extracted estimates of the stiffness constants which are accurate to $\sim 1\%$, using modest system sizes (Sec. 4 and Table I). Via the Coulomb-gas-like notions in Sec. 2.1 and 2.5, the stiffnesses imply critical exponents (see Table II). The latter show that our models belong to new universality classes, and (for the dimer-loop model) the exponents are suggestively close to being simple rational numbers. Each of our models has an anomalous feature: in the dimer-loop model the z_2 height component is smooth yet has critical correlations (Sec. 4.2), and in the noncrossing-dimer model correlation functions are anisotropic even in the critical limit (Sec. 2.5).

In this work, we have tested a new and better Monte Carlo technique for evaluating critical exponents. The results of these simulations (and those of other height models [10,11]) clearly show that the most efficient way to extract K is to measure the Gaussian height fluctuations and use (2.3) with (2.8) and (2.9) (or their generalizations) to infer the exponents, rather than to measure correlation functions directly. Unfortunately, this approach is applicable only to height models (and even spin models which have height representations at $T = 0$ generally do not at $T > 0$.)

We can see this comparison a bit more sharply, because (as discussed in Sec. 4.1) the measured, Fourier-transformed height fluctuations $\langle |\tilde{z}(\mathbf{p})|^2 \rangle$ in fact contain not only the peak around $\mathbf{p} = \mathbf{O}$ from the long wavelength modes, but also peaks around special points on the zone boundary, proportional to the structure factor of a local operator. In other words, as a side-effect we have directly measured (the Fourier transform of) the correlation function of that local operator; thus the singular powers $2 - \eta^{(1)}$ and $2 - \eta^{(2)}$ found around the zone boundary peaks are the best estimates of the exponents that could be obtained by the standard approach. But in fact those peaks were not strong enough to extract meaningful values of the exponents; a larger system size would be necessary. Since the standard analysis using the operator correlation functions uses the *same* data that enter the “height-fluctuation” analysis, this gives a fair measure of the superiority of the latter approach.

It is interesting to compare our methods to another older literature, that of SOS models simulations. These simulations [20] have frequently determined K by fitting the system size dependence of the net height variance W^2 to eq. (4.5). Such a method throws away much of the information in the smallest \mathbf{p} wavevectors by integrating over them. In other cases [21] authors have evaluated the correlation function $C(\mathbf{x})$ fitting to eq. (2.5). This correlation function, in principle, has the same information as $\langle |\tilde{z}(\mathbf{p})|^2 \rangle$, but it does not exclude the large- \mathbf{p} modes (with their systematic errors) quite as cleanly. In either of the two older methods, K would be extracted from a linear fit to the logarithmic dependence. Either of those methods would work poorly for our data, due to the limited range of $\ln r$ offered with system size $L = 32$. With the Fourier method, we can already get the correct stiffness to $\sim 10^{-3}$ (in the simple dimer case, which seems especially favorable).

The dimer-loop model is a good candidate for a Bethe-ansatz exact solution, since it maps to the square-

lattice fully-packed loop (FPL) model with fugacity $n = 2$, while the honeycomb FPL model is soluble [22].

It is also interesting to note that the dimer-loop model is a limiting case of the family of “loop-gas” models, which also arise from the superposition of two dimer coverings. Namely, we this loop-gas has a fugacity for ordinary loops $y = 2$, and a fugacity for loops of length 2 (corresponding to superposed black and white dimers) is $x = 0$. [23] (The original case of the loop gas had $y = 4$ and $x = 2$, and described the correlation functions of the nearest-neighbor resonating-valence bond variational wavefunction for the spin-1/2 antiferromagnet on the square lattice.)

Another promising direction would be to study the “ghost” versions of the two-color dimer models by a Kosterlitz-Thouless type of renormalization group, e.g. to determine how the coupling between colors u renormalizes when it is small.

Acknowledgments

We would like to thank J. K. Burton, J. Kondev, and C. Zeng for discussions. C.L.H. was supported by NSF Grant DMR-9214943. and R.R. by the David and Lucile Packard Foundation.

REFERENCES

- [1] R. Liebmann, 1986, *Statistical Physics of Periodically Frustrated Ising Systems* (Springer Lecture Notes on Physics No. 251).
- [2] J. Kondev and C. L. Henley, *Nuc. Phys. B* 464, 540 (1996) [cond-mat/9511102]; see also J. Kondev and C. L. Henley, *Phys. Rev. Lett.* 74, 4580 (1995), and J. Kondev, in *Proc. Symposium on Exactly Soluble Models in Statistical Mechanics*, (Northeastern Univ., March 1996), ed. C. King and F. Y. Wu.
- [3] C. L. Henley, unpublished.
- [4] See e.g. D. R. Nelson in *Phase Transitions and Critical Phenomena*. ed. C. Domb and J. L. Lebowitz (?) (Academic Press, London, 1983), vol. 7.
- [5] H. W. J. Blöte and H. J. Hilhorst, *J. Phys. A* 15, L631 (1982); B. Nienhuis, H. J. Hilhorst, and H. W. J. Blöte, *J. Phys. A* 17, 3559 (1984).
- [6] D. A. Huse and A. D. Rutenberg, *Phys. Rev. B* 45, 7536 (1992).
- [7] H. W. J. Blöte and B. Nienhuis, *Phys. Rev. Lett.* 72, 1372 (1994).
- [9] N. Read 1992, reported in Kagomé workshop (Jan. 1992), and unpublished.
- [10] J. Kondev and C. L. Henley, *Phys. Rev. B* 52, 6628 (1995).
- [11] C. Zeng and C. L. Henley, unpublished.
- [12] J. K. Burton and C. L. Henley, preprint, to be submitted to *J. Phys. A* (1996).
- [13] J. Kondev and C. L. Henley, *Phys. Rev. Lett.* 74, 4580 (1995)
- [14] B. Nienhuis in *Phase Transitions and Critical Phenomena*, ed. C. Domb and J. L. Lebowitz (Academic Press, London, 1987), vol. 11.
- [15] H. N. V. Temperley and M. E. Fisher, *Phil. Mag.* 6, 1061 (1961); P. W. Kasteleyn, *Physica* 27, 1209 (1961); M. E. Fisher and J. Stephenson, *Phys. Rev.* 132, 1411 (1963); J. Stephenson, *J. Math. Phys.* 5, 1009 (1964).
- [16] See E. H. Lieb and F. Y. Wu 1972, in *Phase Transitions and Critical Phenomena*, ed. C. Domb and M. S. Green, (Academic Press, 1972), vol. 1.
- [17] W. Zheng and S. Sachdev, *Phys. Rev. B* 40, 2704 (1989); L. S. Levitov, *Phys. Rev. Lett.* 64, 92 (1990); L. B. Ioffe and A. I. Larkin, *Phys. Rev. B* 40, 6941 (1989).
- [18] H. van Beijeren, *Phys. Rev. Lett.* 38, 993 (1977).
- [19] C. L. Henley, submitted to *J. Stat. Phys.*
- [20] H. G. Evertz, M. Hasenbusch, M. Marcu, K. Pinn, and S. Solomon, *J. Phys. (France) I* 1, 1669 (1991).
- [21] W. J. Shugard, J. D. Weeks, and G. H. Gilmer, *Phys. Rev. Lett.* 41, 1399 (1978);
- [22] M. T. Batchelor, J. Suzuki, and C. M. Yung, *Phys. Rev. Lett.* 73, 2646 (1994).
- [23] B. Sutherland, *Phys. Rev. B* 38, 6855 (1988), and unpublished.

FIGURE CAPTIONS

Fig. 1. Sample configurations of the models from simulations of 8×8 lattice: (a). Simple dimer model, heights $z(\mathbf{x})$ marked; (b). dimer-loop model, with $z_2(\mathbf{x})$ marked; (c). the same loops (dimer colors not distinguished) with arrows showing the mapping to the 6-vertex model, and height component z_1 marked; (d). noncrossing-dimer model.

Fig. 2. Rearrangements between two microstates; the first four form the basis of Monte Carlo updates (see Sec. 3). (a). Simple dimer model, showing the heights $z(\mathbf{x})$. (b,c) Two-color dimer-loop covering, showing heights $z_2(\mathbf{x})$. (d,e). Two-color noncrossing-dimers covering. (f). Fragment of a state in the noncrossing-dimer model which cannot be updated. Rearrangements (a,b,d) produce the smallest possible difference between ground states.

Fig. 3. Ideal states (a). for simple dimer model, (b) for dimer-loop model, (c). also for dimer-loop model (alternative candidate ideal state) and (c). for noncrossing-dimer model. In (d), part of a “roof” configuration is shown for the noncrossing-dimer model; this is the opposite of an ideal state, since it has maximum height gradients.

dimer-loop... when I eyeball the curves, I get $0.76 \pm .02$, and it is easier to believe it deviates up rather than down. So I’ll bet for 0.785.

Fig. 4. Graph of ideal states in height space (heavy dots). The dashed grid marks the ideal states of the ghost (noninteracting) two-color dimer models. Rotated axes are indicated corresponding to the even and odd combinations of (h_B, h_W) which appear in the elastic free energy (see Sec. 2.4). (a). Simple dimer model (b). Dimer-loop model (c). Noncrossing-dimer model.

Fig. 5. Simple dimer model results. $[P(\mathbf{p})^2 \langle |\tilde{z}(\mathbf{p})|^2 \rangle]^{-1}$ is plotted against the squared wavevector $|\mathbf{p}|^2$; where $\tilde{z}(\mathbf{p})$ is the Fourier transform of the configuration of heights. (Here $P(\mathbf{p})^2 \approx |\mathbf{p}|^2$ near $|\mathbf{p}| = 0$, see text). In light of eq. (2.3), the graph should approach a constant near $|\mathbf{p}| = 0$. In order to test the isotropy in real space, we show data for wavevectors \mathbf{p} along (10) and (11) directions by filled and open circles, respectively.

Fig. 6. BCSOS model results, using the same conventions as in Fig. 5.

Fig. 7. Dimer-loop results (a). Rough component z_1 , using the conventions of Fig. 5. (b). Anomalously smooth component z_2 , using log-log plot to check power law behavior.

Fig. 8. Noncrossing-dimer results Here data for wavevectors along the $(1, -1)$ axis must be distinguished from those along $(1, 1)$ axis. The limit at $\mathbf{p} \rightarrow 0$ is expected to be a function of direction $\hat{\mathbf{p}}$ in this model.

0	3	0	-1	0	3	4	3
1	2	1	2	1	2	5	2
4	3	0	3	4	3	4	3
5	2	1	2	1	2	1	2
4	3	4	3	0	3	4	3
5	2	1	2	1	2	5	2
4	3	0	-1	0	3	4	3
1	2	1	2	1	2	5	2

Figure 1(a)

1	1	1	1	1	2	1	1
1	2	2	2	1	1	1	2
1	1	1	2	2	1	2	2
2	2	1	1	1	1	1	2
1	1	1	2	1	2	1	1
2	2	1	2	1	2	2	2
1	2	1	1	1	2	1	1
1	2	2	2	2	2	1	4

Figure 1(b)

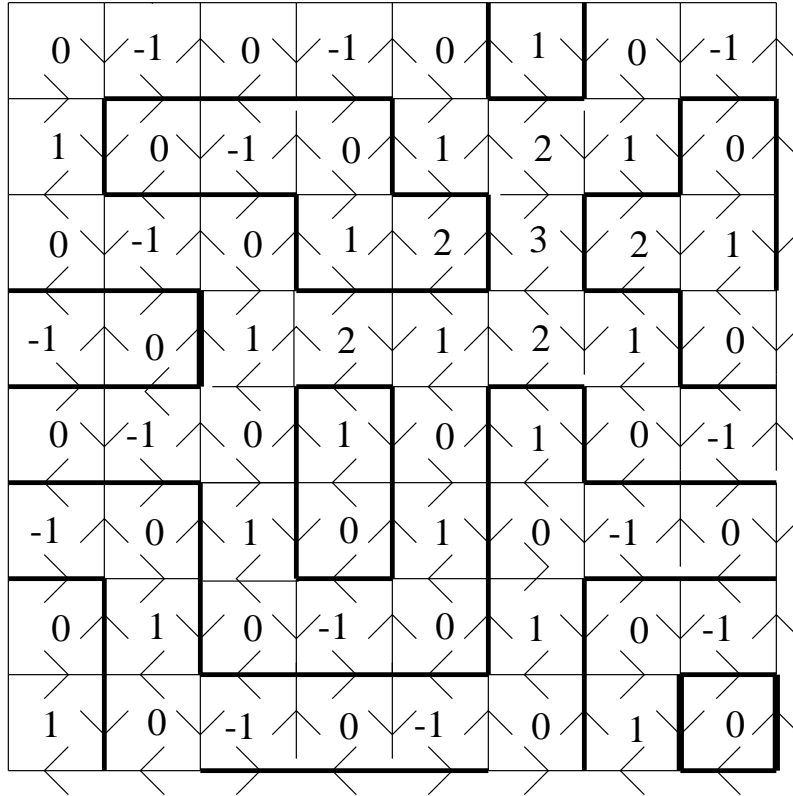


Figure 1(c)

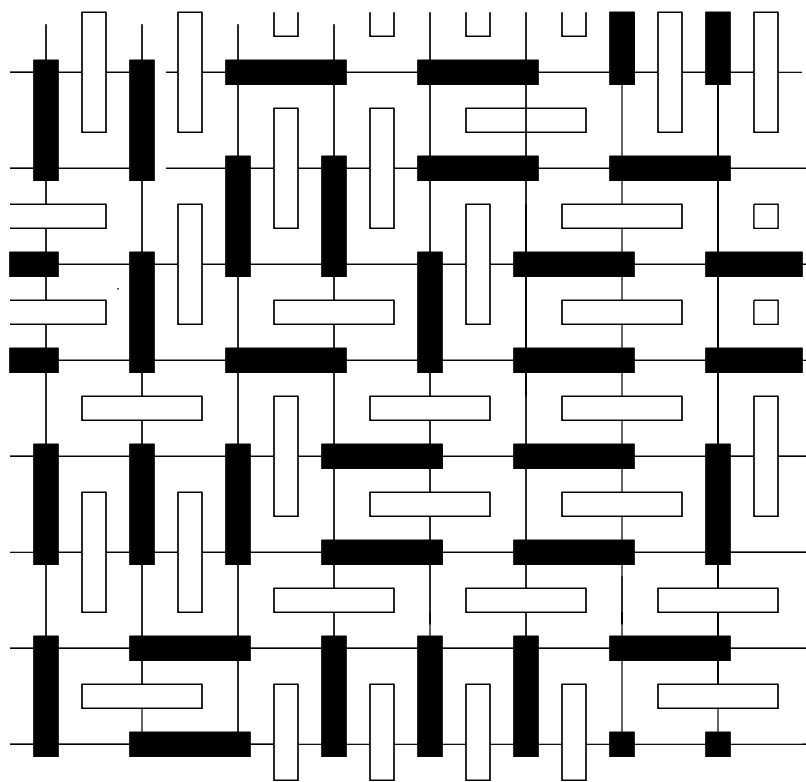


Figure 1(d): Non-crossing dimers

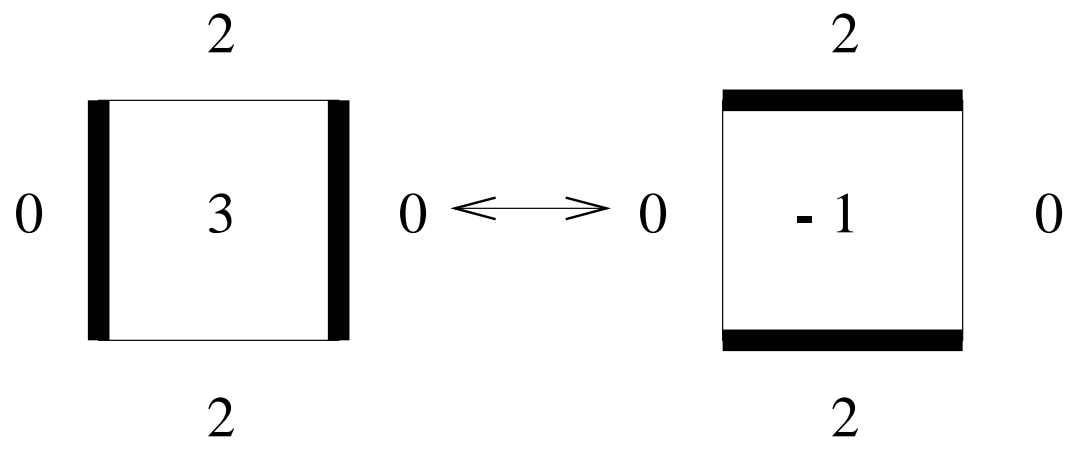


Figure 2(a): Simple dimer model

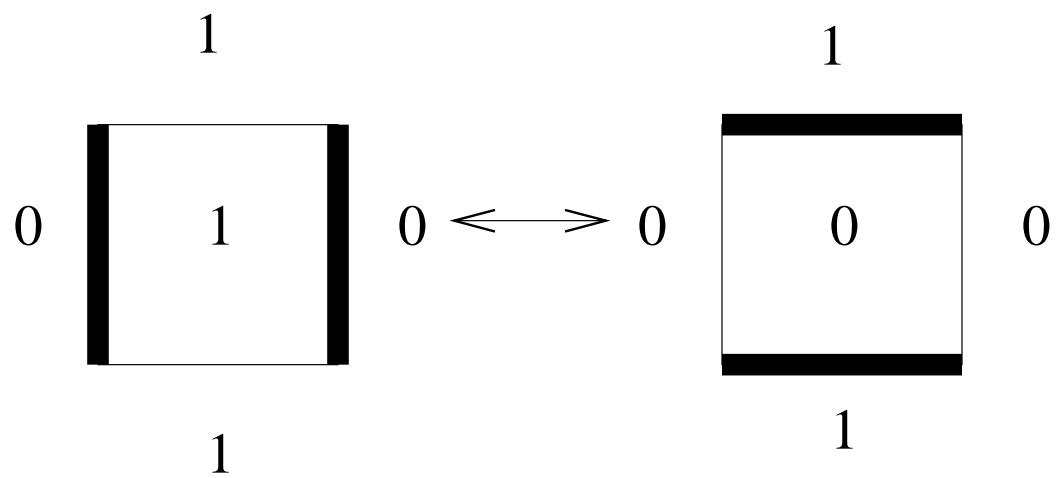


Figure 2(b): Dimer loop covering

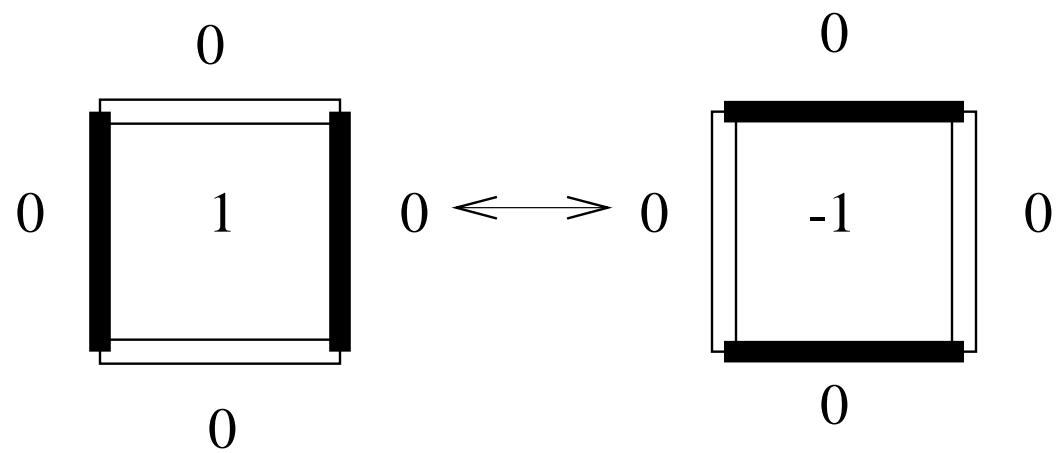


Figure 2(c): Dimer loop covering

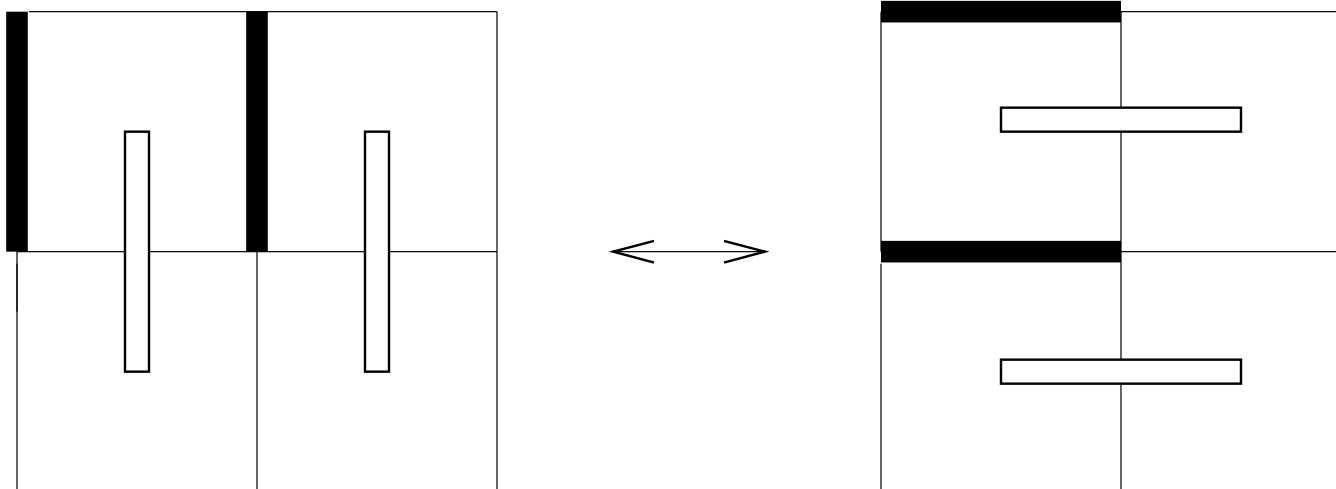


Figure 2(d): Two-colour non-crossing dimer covering

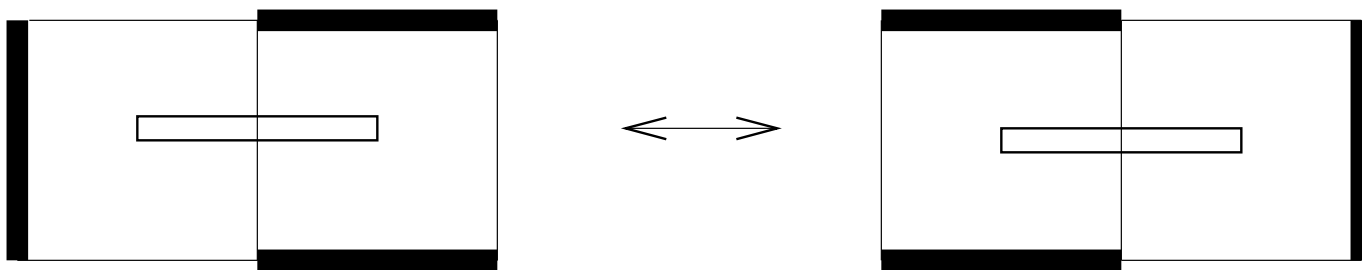


Figure 2(e): Two-color non-crossing dimer covering

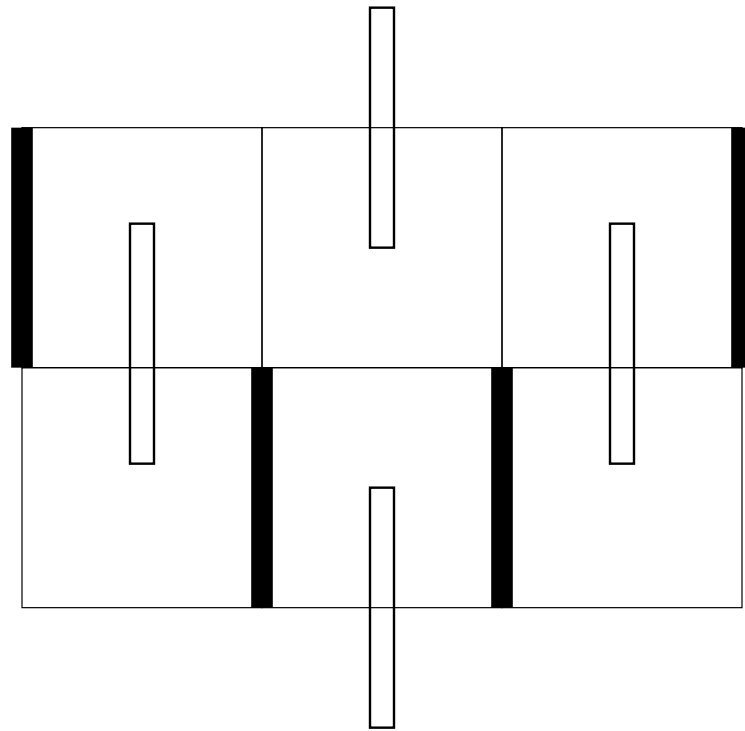


Figure 2(f): Two-color non-crossing dimer covering

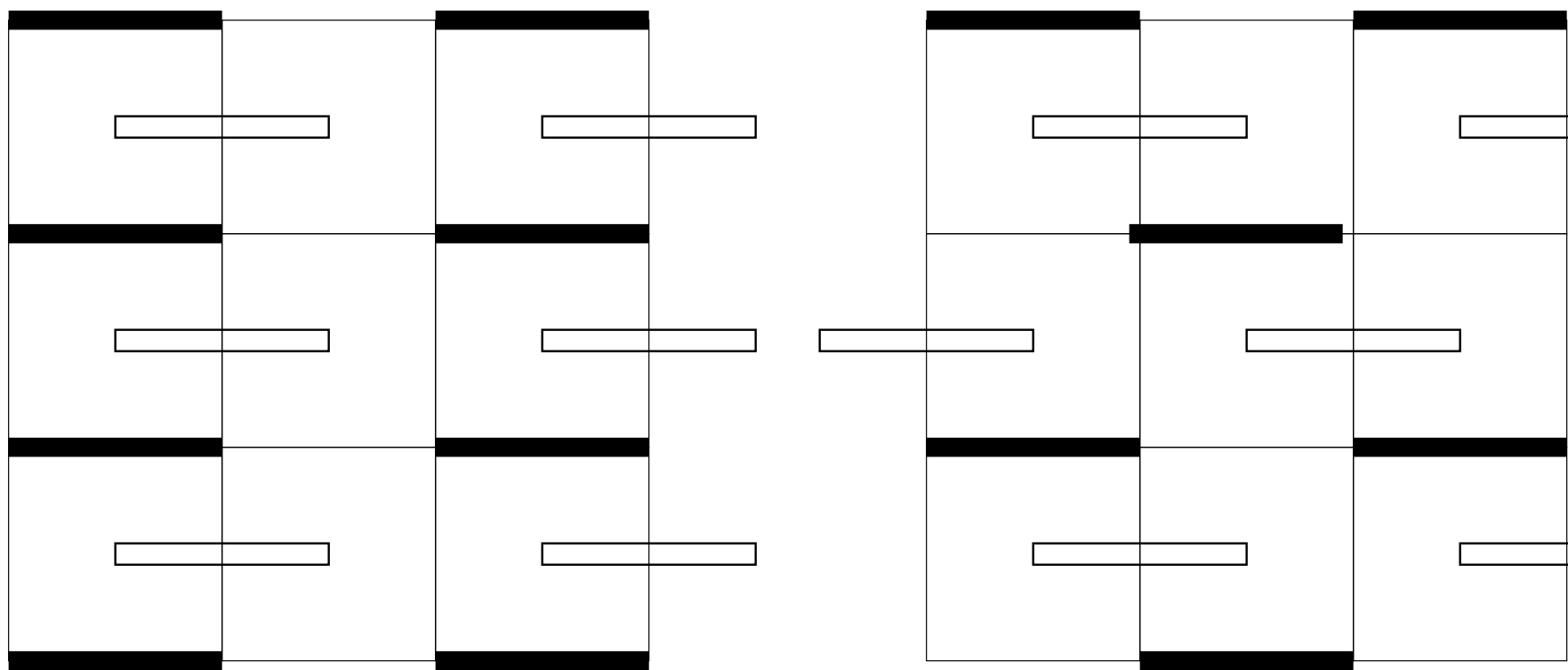
0	1	0
3	2	3
0	1	0

(a) Simple dimer model

1	1	1
0	0	0
1	1	1

(b) Dimer loop model

Figure 3



(c) and (d): Non-crossing dimer model

Figure 3

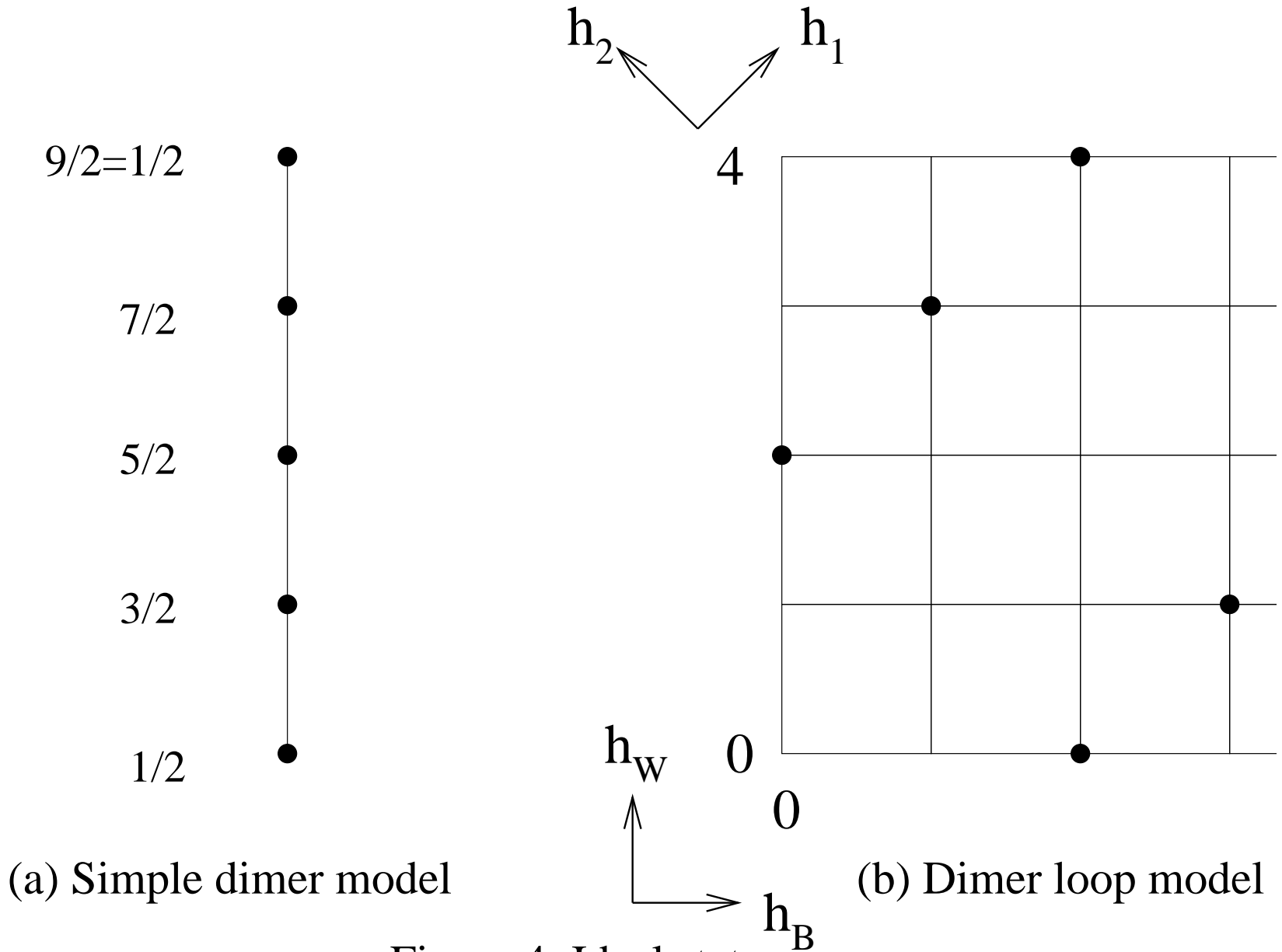


Figure 4: Ideal states

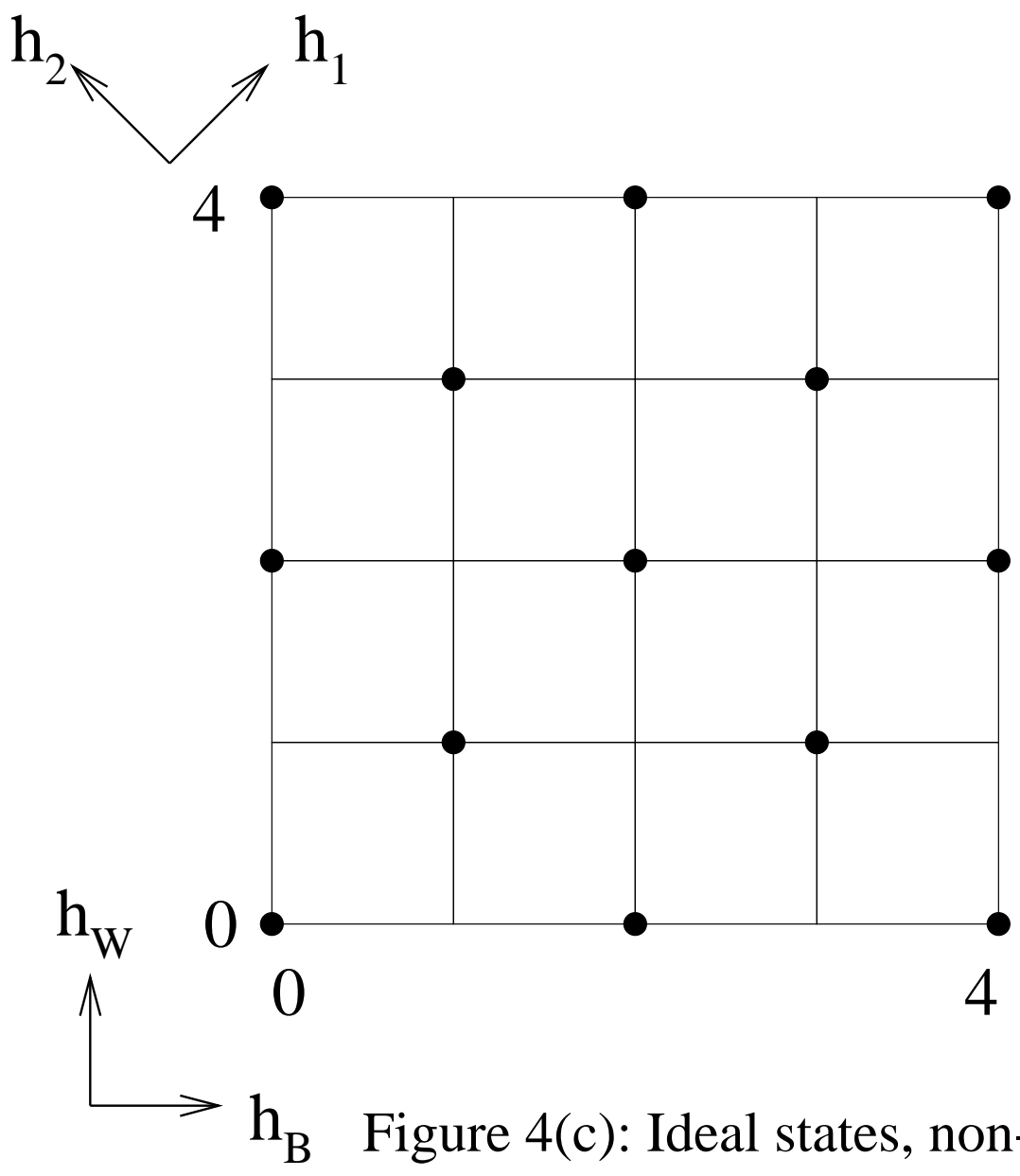
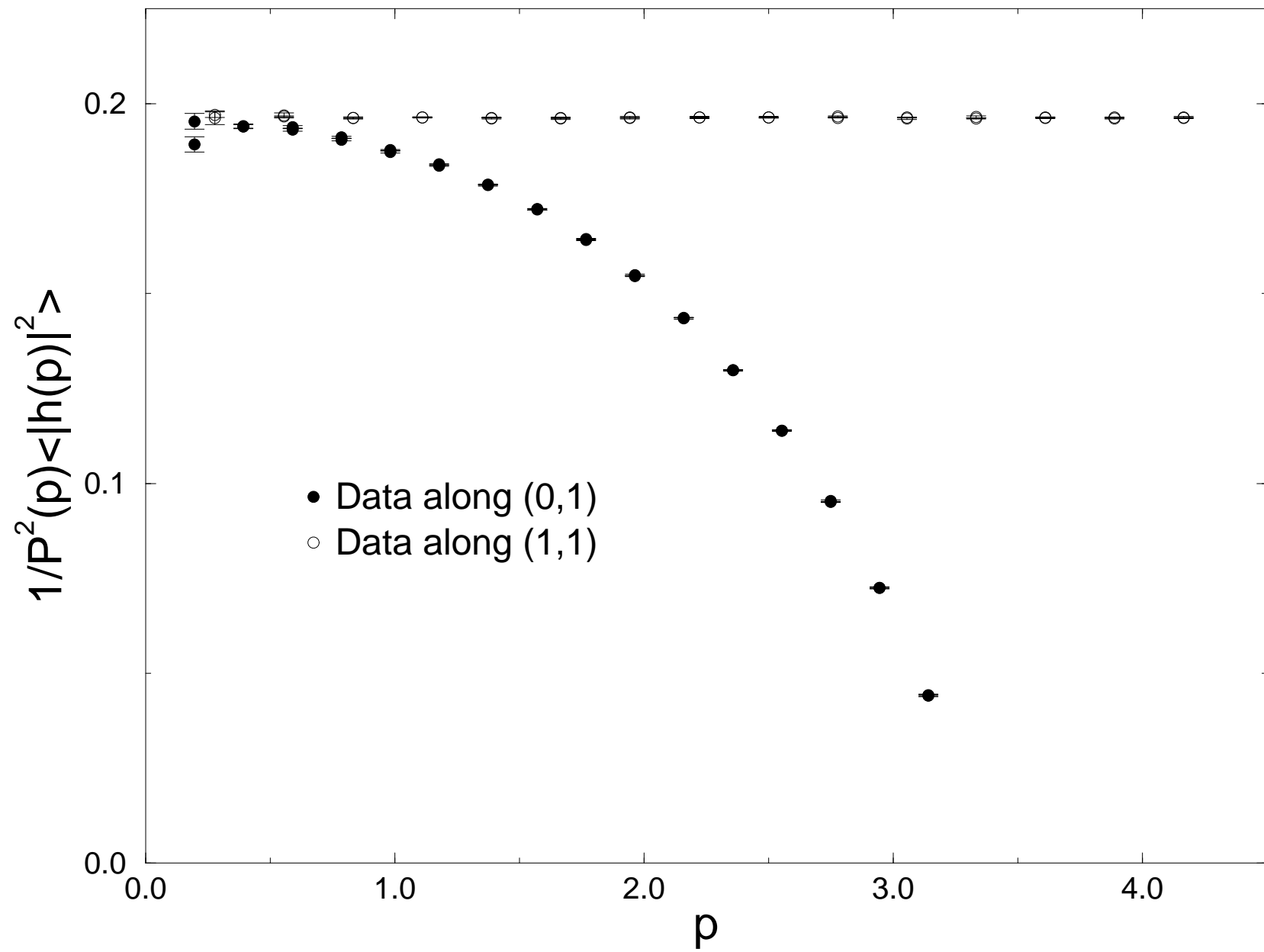
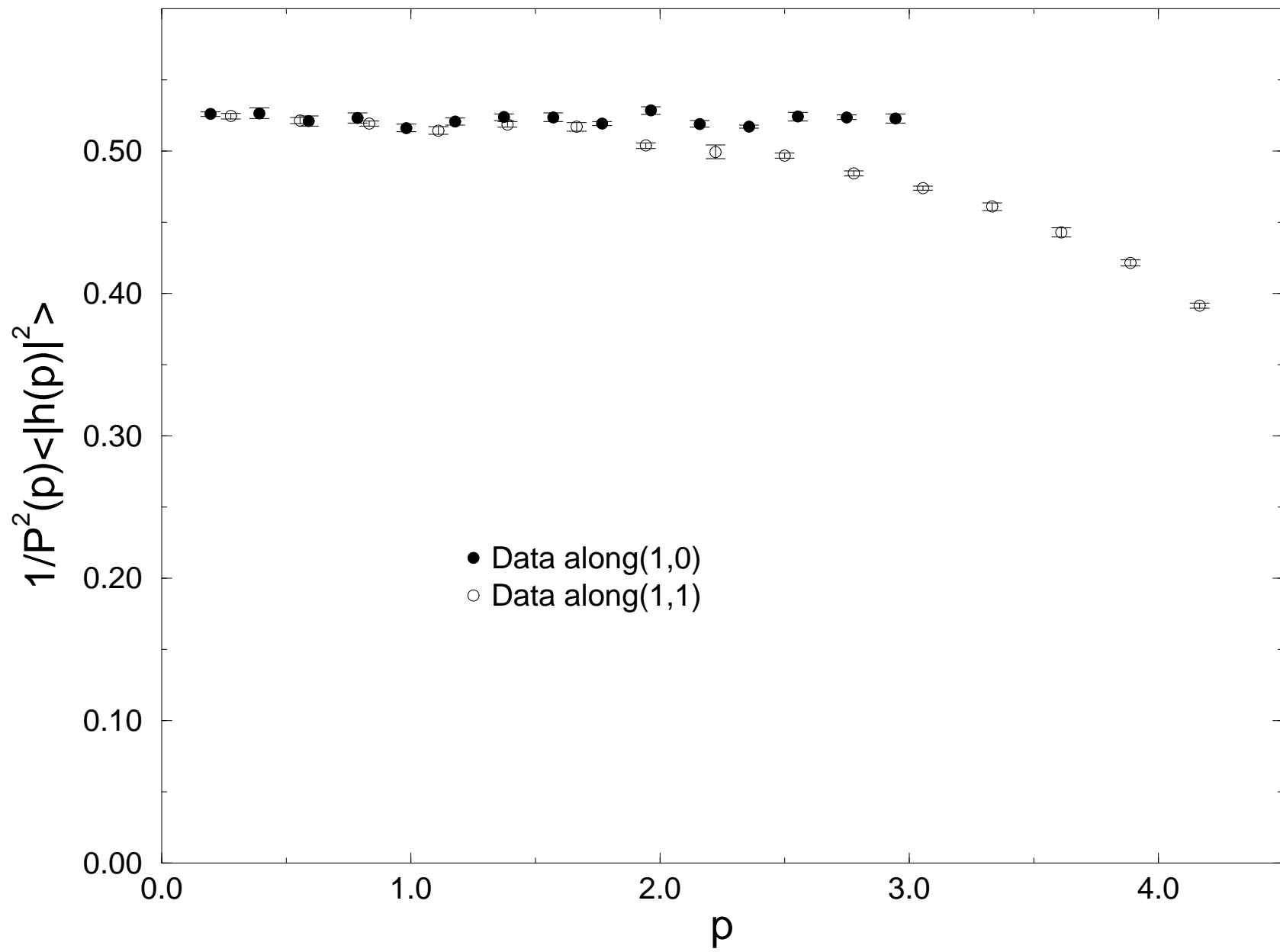
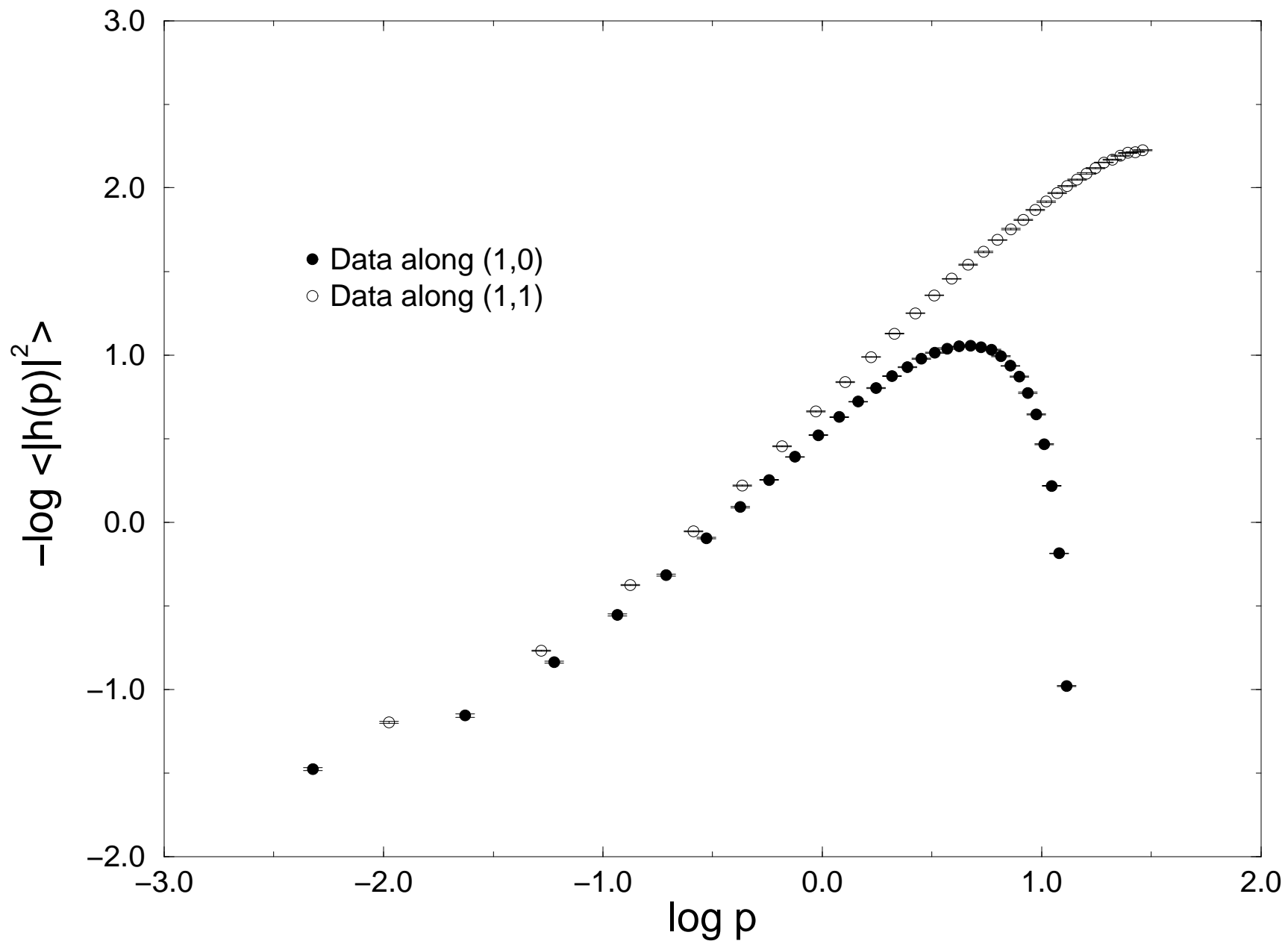
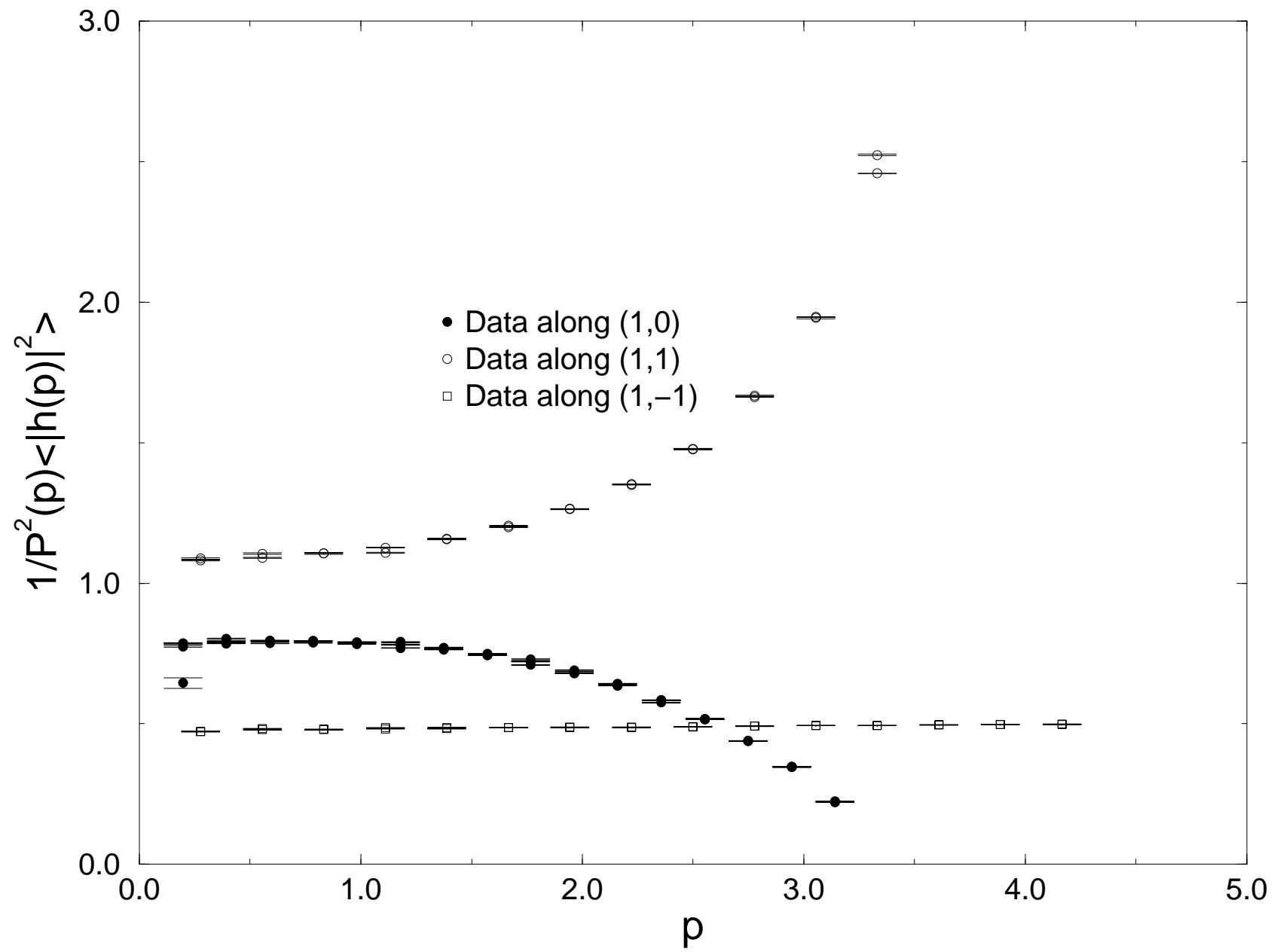


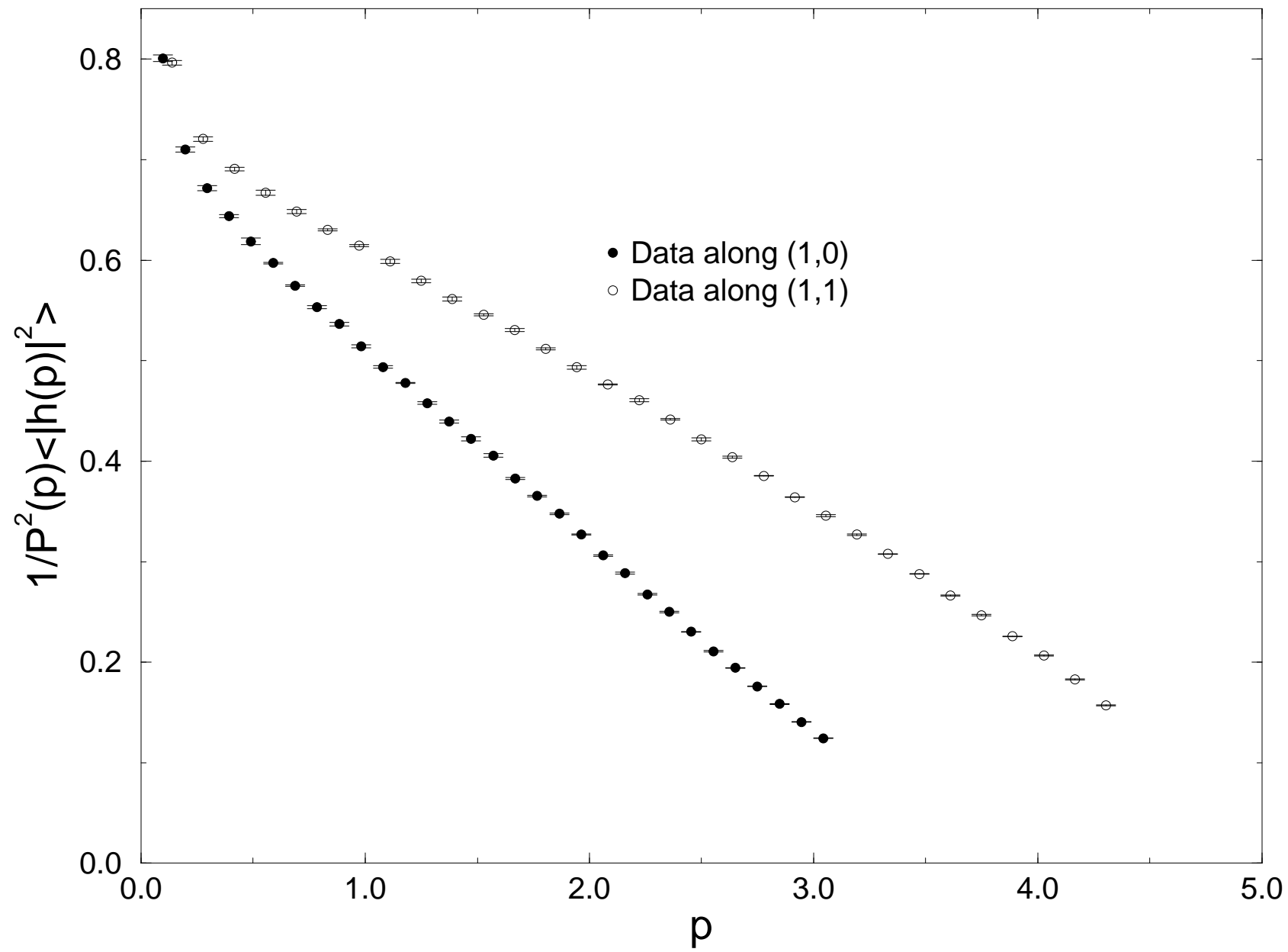
Figure 4(c): Ideal states, non-crossing dimer model











TABLES

TABLE I. Stiffness constants

Model	L	Constants	Exact values
BCSOS	30	$K = 0.513(0.013)$	$\pi/6 = 0.523^a$
Simple dimer	32	$K_0 = 0.1959(0.0007)$	$\pi/16 = 0.1963^a$
Dimer-loop	64	$K_1 = 0.745(.015)$ $K_2 = \infty$	$\pi/4 = 0.785?$ ∞
Noncrossing-dimer	32	$K_+ = 0.273(.006)$ $K_- = 0.118(0.005)$	$\pi/12 = 0.2618?$ $\pi/27 = 0.1164?$

^a Known from an exact solution.

TABLE II. Proposed critical exponents

Model	\mathbf{G}^\perp	$\eta(\mathbf{G}^\perp)$	\mathbf{b}	$\eta_v(\mathbf{b})$
BCSOS	$2\pi/2^a$	3	2	$\frac{1}{3}$
Simple dimer	$2\pi/4^a$	2	4	$\frac{1}{2}$
Dimer-loop	$(2\pi/4, 0)^b$	$\frac{1}{2}?$	(4,0)	2?
Noncrossing-dimer	$2\pi/4(1/\sqrt{2}, 1/\sqrt{2})^b$	$\frac{9}{4}?$	(2, 2)	$\frac{4}{9}?$

^a Spin models (the 3-state Potts antiferromagnet for the BCSOS case, and the fully frustrated square lattice Ising model in the simple dimer case) are represented by the same height model, except that they have a larger repeat spacing in height space (3 times larger or 2 times larger for the respective cases). Thus spin-spin correlations have $\eta = 1/3$ for the 3-state Potts model, or $1/2$ for the fully frustrated Ising model, on the square lattice.

^b For two-color cases, (G_1, G_2) is given.